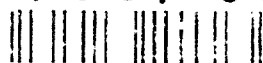
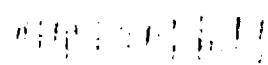


AD-A267 656



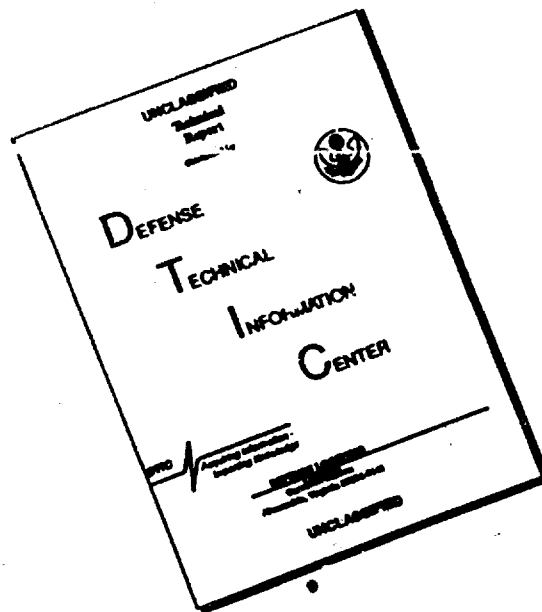
AD

9313542



**BEST
AVAILABLE COPY**

DISCLAIMER NOTICE



**THIS DOCUMENT IS BEST
QUALITY AVAILABLE. THE COPY
FURNISHED TO DTIC CONTAINED
A SIGNIFICANT NUMBER OF
PAGES WHICH DO NOT
REPRODUCE LEGIBLY.**

REPORT DOCUMENTATION PAGE			Form Approved OMB No. 0704-0188	
<small>1. AGENCY USE ONLY (Leave blank)</small>				
2. REPORT DATE May 1993		3. REPORT TYPE AND DATES COVERED THESIS/DISSEMINATION		
4. TITLE AND SUBTITLE An Experimental Investigation of the Effects of Leading Edge Geometry on the Dynamics of Blunt Fin-Induced Shock Wave Turbulent Boundary Layer Interaction			5. FUNDING NUMBERS	
6. AUTHOR(S) Kelly Kleifges				
7. PERFORMING ORGANIZATION NAME(S) AND ADDRESS(ES) AFIT Student Attending: The Univ of Texas At Austin			8. PERFORMING ORGANIZATION REPORT NUMBER AFIT/CI/CIA- 93-093	
9. SPONSORING MONITORING AGENCY NAME(S) AND ADDRESS(ES) DEPARTMENT OF THE AIR FORCE AFIT/CI 2950 P STREET WRIGHT-PATTERSON AFB OH 45433-7765			10. SPONSORING MONITORING AGENCY REPORT NUMBER	
11. SUPPLEMENTARY NOTES				
12a. DISTRIBUTION AVAILABILITY STATEMENT Approved for Public Release IAW 190-1 Distribution Unlimited MICHAEL M. BRICKER, SMSgt, USAF Chief Administration			12b. DISTRIBUTION CODE	
13. ABSTRACT (Maximum 200 words)				
14. SUBJECT TERMS			15. NUMBER OF PAGES 81	
			16. PRICE CODE	
17. SECURITY CLASSIFICATION OF REPORT	18. SECURITY CLASSIFICATION OF THIS PAGE	19. SECURITY CLASSIFICATION OF ABSTRACT	20. LIMITATION OF ABSTRACT	

AN EXPERIMENTAL INVESTIGATION OF THE EFFECTS OF LEADING
EDGE GEOMETRY ON THE DYNAMICS OF BLUNT FIN-INDUCED
SHOCK WAVE TURBULENT BOUNDARY LAYER INTERACTION

APPROVED:

DSI ollens
David J. Bogard

Copyright
by
Kelly Kleifges
1993

**AN EXPERIMENTAL INVESTIGATION OF THE EFFECTS OF LEADING
EDGE GEOMETRY ON THE DYNAMICS OF BLUNT FIN-INDUCED
SHOCK WAVE TURBULENT BOUNDARY LAYER INTERACTION**

by

KELLY KLEIFGES, B.S.

THESIS

Presented to the Faculty of the Graduate School of
The University of Texas at Austin
in Partial Fulfillment
of the Requirements
for the Degree of

MASTER OF SCIENCE IN ENGINEERING

THE UNIVERSITY OF TEXAS AT AUSTIN

May 1993

DTIC QUALITY INSPECTED 12

Availability Codes	
DTIC TAB	
Unannounced	
Justification	
By	
Distribution	
Availability Codes	
Dist	Availability for Special
A-1	

ACKNOWLEDGMENTS

The author would like to express his gratitude to Dr. David S. Dolling for his guidance and support throughout the course of this work. Special thanks also go to Mehmet Erengil, Leon Brusniak, Edward Zihlman Jr. and Frank Wise for varied technical support.

This study was funded largely by NASA Langley Grant NAG 1-1005 and monitored by Dr. William E. Zorumski. The student was supported as a salaried employee of the United States Air Force. These sources of support are gratefully acknowledged.

April 1993

ABSTRACT

AN EXPERIMENTAL INVESTIGATION OF THE EFFECTS OF LEADING EDGE GEOMETRY ON THE DYNAMICS OF BLUNT FIN-INDUCED SHOCK WAVE TURBULENT BOUNDARY LAYER INTERACTION

by

KELLY KLEIFGES, B.S.

Supervisor: Dr. DAVID S. DOLLING

Fluctuating wall pressure measurements have been made on centerline upstream of blunt fins in a Mach 5 flow. Standard time series analysis and conditional sampling algorithms have been used to examine the effects of leading edge sweep, leading edge shape, and fin root modifications on the RMS level and spectral content of fluctuating pressures. Results show that the fluctuating loads can be reduced significantly by appropriate modification of the fin leading edge. Leading edge sweep considerably reduces the mean and RMS pressure loading at the fin root, the extent of the region of unsteady separation shock motion (i.e. the intermittent region), and the separation length. The spectral content of pressure fluctuations in the intermittent region shifts to higher frequencies with leading edge sweep, while the spectral content of pressure fluctuations in the separated region is virtually unchanged by leading edge sweep. Of the different fin leading edge

geometries which induce the same size interaction, the "blunter" configurations produce smaller intermittent regions and larger separated regions. While the use of a strake at the fin leading edge root has virtually no effect, a swept hemicylindrically blunted root fillet reduces the centerline upstream influence and intermittent region length by 50%, and reduces the mean and RMS pressure loading at the fin root by 75% and 95% respectively.

TABLE OF CONTENTS

Section	Page
ACKNOWLEDGMENTS	iv
ABSTRACT	v
LIST OF TABLES	x
LIST OF FIGURES	xi
NOMENCLATURE	xv
1 INTRODUCTION	1
1.1 Background	1
1.2 Objectives	3
2 LITERATURE REVIEW	5
2.1 Introduction	5
2.2 General Characteristics	6
2.2.1 Flow Structure and Length Scales	6
2.2.2 Mean and RMS pressure Distributions	8
2.2.3 Effect of Leading Edge Sweep	9
2.2.4 Application of Computational Fluid Dynamics	10
2.3 Mean Flow Field Structure	10
2.4 Unsteadiness of Shock Wave Turbulent Boundary Layer Interactions	11
2.4.1 General	11
2.4.2 Quantification of the Unsteadiness	14

2.4.3	Mechanisms of the Unsteadiness	15
2.5	Summary	18
3	EXPERIMENTAL PROGRAM	19
3.1	Wind Tunnel	19
3.2	Experimental Methods	20
3.2.1	Surface Tracer Flow Visualization Method	20
3.2.2	Fluctuating Wall Pressure Measurement	20
3.3	Models	22
3.4	Test Program	24
4	ANALYSIS TECHNIQUES	25
4.1	General Time Series and Statistical Analysis	25
4.2	Conditional Sampling	25
4.2.1	Shock Statistics Algorithm	25
4.2.2	Separation Shock Foot Position and Velocity Histories	27
4.2.3	Calculation of Interaction Length Scales	28
5	DISCUSSION OF RESULTS	29
5.1	Effects of Leading Edge Sweep	29
5.1.1	Mean and RMS Pressure Distributions	29
5.1.2	Flow Length Scales	30
5.1.3	Zero-Crossing Frequency and Power Spectral Density Distributions	31
5.1.4	Summary of Effects of Leading Edge Sweep	32
5.2	Effects of Changes in Leading Edge Shape	33

5.2.1	Mean and RMS Pressure Distributions.....	33
5.2.2	Flow Length Scales.....	33
5.2.3	Power Spectral Density Distributions	34
5.2.4	Summary of the Effects of Leading Edge Shape	34
5.3	Leading Edge Modifications	35
5.3.1	Filletted Fin Root	35
5.3.2	Unswep Fin with Strake Modification.....	35
5.4	Flow Physics	36
5.4.1	Cross-correlations of Signals from Adjacent Transducers	36
5.4.2	Correlation of Signals Upstream and Downstream of Separation	37
6	CONCLUSIONS	39
	REFERENCES	41
	FIGURES.....	45
	VITA	82

LIST OF TABLES

Table	Title	Page
3.1	Freestream Flow Conditions	19
3.2	Boundary Layer Properties (McClure, 1991).	20

LIST OF FIGURES

Figure	Title	Page
1.1	General Characteristics of Fin-Induced Shock Wave Turbulent Boundary Layer Interaction (Blank, 1993)	45
2.1	Mean and RMS Pressure Distributions on Centerline Upstream of Blunt Fins at Mach 3 and Mach 5 (Dolling, 1993)	46
2.2	Computed Pressure Distribution at Mach 3 (a) Centerline; (b) Fin Leading Edge (Hung and Buning, 1985)	47
2.3	Mean Flow Field Structure (Avduevskii and Medvedev, 1967)	48
2.4	Computed Particle Paths in the Plane of Symmetry, (a) Mach 3 Hemicylindrically Blunted Fin (Hung and Buning, 1985), (b) Mach 5 Flat Faced Fin (Hung 1989)	49
2.5	Samples of Pressure Time Histories Upstream of Fin on Centerline (Dolling and Bogdonoff, 1981)	50
2.6	Wall Pressure Probability Density Distributions Upstream of Fin on Centerline (Dolling and Bogdonoff, 1981)	51
2.7	Power Spectral Density Distributions on Centerline in Mach 5 Blunt Fin Interactions (Brusniak and Dolling, 1992)	52
2.8	"Skirt" Fin Root Modification (Blank 1992)	53
2.9	Maximum Shock Zero Crossing Frequency as a Function of Intermittent Region Length for all Model Configurations (Gonzalez and Dolling, 1993).....	54

2.10	Mean Shock Velocity Normalized by Freestream Velocity as a Function of Intermittent region Length for all Model Configurations (Gonsalez and Dolling, 1993)	55
2.11	Effect of Cylinder Diameter and Boundary Layer Thickness on Power Spectra at Maximum RMS near Separation in Mach 5 Interactions (Dolling and Smith, 1989)	56
2.12	Correlation of Power Spectra at Maximum RMS near separation using L_i as a Scale for the Reduced Frequency (Gonsalez and Dolling, 1993)	57
2.13	Ensemble-averaged Wall Pressure Histories for (a) 3-channel Downstream Sweep, (b) 3-channel Upstream Sweep (trigger on Channel 7) (McClure, 1992)	58
3.1	Swept Hemicylindrically Blunted Fins and Wedge Shaped Leading Edge Fin	59
3.2	Flat Faced Fin	60
3.3	Swept Hemicylindrically Blunted Fillet	61
3.4	Strake Modification to Unswept Fin Root	62
4.1	Application of the Two-Threshold Algorithm (Brusniak 1991)	63
4.2	Conversion of Boxcar Signals to $X_s(t)$ and $V_s(t)$ (Erengil, 1992)	64
5.1	Variation of Mean Pressure with Leading Edge Sweep	65
5.2	Variation of RMS Pressure with Leading Edge Sweep	66
5.3	Variation of Flow Length Scales with Leading Edge Sweep	67
5.4	Variation of Zero-Crossing Frequency with Leading Edge Sweep	68

5.5	Dimensional and Normalized Power Spectral Density Distributions at 50% Intermittency	69
5.6	Dimensional and Normalized Power Spectral Density Distributions in the Separated Region	70
5.7	Dimensional and Normalized Power Spectral Density Distributions at the Fin Root	71
5.8	Mean and RMS Pressure Distributions for Three Interactions with the Same Upstream Influence	72
5.9	Variation of Flow Length Scales with Leading Edge Geometry	73
5.10	Dimensional and Normalized Power Spectral Density Distributions at 50% Intermittency	74
5.11	Dimensional and Normalized Power Spectral Density Distributions in the Separated Region	75
5.12	Dimensional and Normalized Power Spectral Density Distributions at the Fin Root	76
5.13	Flow Visualization Results for Unswept Hemicylindrically Blunted Fin and Unswept Fin with Fillet Root Modification	77
5.14	Mean and RMS Pressure Distribution for the Hemicylindrically Blunted Fillet	78
5.15	Cross Correlation of Fluctuating Pressure Measurements from Adjacent Transducers in the Separated Region	79
5.16	Cross-correlation of Adjacent Transducers at the same Relative Location in three Different Interactions	80

5.17	Cross-correlation of Signals From Upstream and Downstream of Separation	81
------	--	----

NOMENCLATURE

C_f	Skin friction coefficient
f_c	Separation shock zero-crossing frequency
L_i	Intermittent region length
L_{sep}	Separation length
L_{ui}	Upstream influence length
M_∞	Freestream Mach number
P_0	Stagnation pressure
P_∞	Freestream static pressure
P_M, P_{max}	Maxima in mean pressure distribution
P_{R1}, P_{R2}, P_{R3}	Maxima in RMS pressure distribution
$\overline{P_w}$	Mean pressure
\overline{P}_{w0}	Boundary layer pressure as calculated by conditional sampling algorithm
Re	Reynolds number
'S'	Separation line
t	Fin thickness
T_0	Stagnation temperature
t_r, t_f	Shock rise and fall times
T_1, T_2	Pressure thresholds used in conditional sampling algorithm
'UI'	Upstream influence line
$V_s(t)$	Shock velocity history
V_∞	Freestream velocity

$V1, V2, V3$	Characteristic velocities from cross-correlations
$X_s(t)$	Shock position history
γ	Intermittency
λ_{LE}	Fin leading edge sweep angle
δ_o	Boundary layer thickness
δ^*	Boundary layer displacement thickness
Π	Boundary layer wake strength parameter
σ_p	RMS of pressure fluctuations
$\sigma_{p_{w0}}$	Boundary layer RMS pressure as calculated by conditional sampling algorithm
θ	Boundary layer momentum thickness
ζ	Center to center distance between adjacent transducers

CHAPTER 1

INTRODUCTION

1.1 Background

One of the many aerodynamic problems associated with supersonic and hypersonic flows around complex airframe geometries is the shock wave boundary layer interaction. Such an interaction can be generated by a large number of configurations including wing-body junctions, inlets, or deflected control surfaces. The aerothermodynamic problems associated with the interactions include very high amplitude unsteady pressure loading and intense local heating rates. For example loading levels of up to 185 dB or more have been measured (Zorumski, 1987). Such high fluctuating loads combined with high temperatures can reduce the fatigue lifetime of conventional structures by orders of magnitude (Dolling 1993). As with most separated flows, shock wave turbulent boundary layer interactions also degrade performance, whether it be due to added drag in external flows or decreased engine efficiency in internal flows.

The use of computational fluid dynamics (CFD) as a design tool is becoming more common in this era of increasing computational power accompanied by decreasing costs. At this time, however, although the mean field is reasonably well reproduced for many flows, the unsteady behavior is not modeled, and thus fluctuating loads cannot be predicted in numerical calculations. Some improvement in the understanding of the exact role of the turbulent fluctuations in the incoming boundary layer and how fluctuations are fed upstream through the separated region is needed before appropriate computational modeling strategies can be developed.

Experimental investigations of supersonic sharp fin, blunt fin, and compression corner flows have been made by many researchers to observe the interactions and attempt to explain the physics of the unsteady phenomena. Recent reviews of the mean and fluctuating properties are given by Settles and Dolling (1990) and Dolling (1993), respectively. There is now sufficient understanding of many of these flows that the adverse effects of these interactions might be controlled, or reduced to some extent, by appropriate design.

The current study, which is experimental, concentrates on the blunt fin-induced shock wave turbulent boundary layer interaction, which most closely resembles that occurring at a wing-body intersection on an aircraft. In such an interaction a large-scale, three-dimensional, separated flow region is generated whose scales are controlled, to first order, by the fin thickness, t (Dolling and Bogdonoff, 1981). Some of the salient features of this interaction are shown in Figure 1.1. The bow shock formed in front of the fin is bifurcated and has the characteristic "λ-foot" shape. Separation is noted by the line marked 'S' and 'UI' is the upstream influence line, the upstream limit of the unsteady separation shock foot travel. The distance between these two lines, L_i , is the intermittent region length, so named because of the intermittent nature of fluctuating pressures measured there. High speed schlieren photography (Degrez, 1981; Blank, 1993) and wall pressure fluctuations (Erengil and Dolling, 1990; Brusniak, 1991; Dolling and Brusniak, 1992; McClure, 1992; Gonzalez and Dolling, 1993) show that the separation process and resulting flowfield are unsteady, generating high amplitude fluctuating pressure loads.

The focus of the present research is to control, or at least influence favorably, the unsteady separation process. This includes reducing overall fluctuating load levels, altering their spectral content, and in the process hopefully reducing the surface area exposed to high loading levels. Having some understanding of the mechanisms that drive the unsteadiness of the separation process is obviously a prerequisite to success. To date, work in blunt fin-induced interactions has shown that turbulent fluctuations in the incoming boundary layer and in the recirculating flow play a role in driving the separation shock motion (Brusniak 1991). The relative importance of each is currently being investigated by Brusniak at the University of Texas at Austin (Brusniak 1993).

1.2 Objectives

The current experimental program was designed to determine whether the dynamics of the separation shock and the turbulent recirculating fluid downstream of the separation shock wave are independent of, or dependent on, the shock generator leading edge geometry. If the separation shock dynamics do depend on leading edge geometry the question arises as to whether fin leading edge shape changes can alter the shock dynamics favorably, and ultimately, through what physical process they effect any changes in the flowfield. Thus the specific objectives of this research are as follows:

- (i) Determine the effect of leading edge sweep and leading edge shape on the unsteadiness of blunt fin-induced shockwave turbulent boundary layer

interactions through investigation of the statistical properties of centerline fluctuating wall pressure measurements,

- (ii) Determine whether minor modifications to the unswept blunt fin configuration can favorably influence the unsteadiness of the shockwave turbulent boundary layer interaction.

In addition, an exploratory attempt was made to determine whether differences in the separated region dynamics caused by the various leading edge changes cause the observed differences in separation shock dynamics.

CHAPTER 2

LITERATURE REVIEW

2.1 Introduction

Boundary layer separation upstream of semi-infinite blunt fins in supersonic flows has been a subject of research in aerodynamics for more than thirty years. Early work concentrating on laminar boundary layer separation induced by blunt fins indicated that the process was steady. Since then unsteady supersonic laminar boundary layer separation has also been reported (Ozcan and Holt, 1984); however, it is not clear whether the unsteadiness is actually due to a transitional shear layer or root vortex, rather than some natural instability (Dolling, 1993).

An equally intriguing problem with more practical applications is the separation of supersonic *turbulent* boundary layers upstream of blunt fins. The mean properties of this type of shock wave boundary layer interaction were documented almost thirty years ago by Voitenko (1967) for unswept fins, and by Price and Stallings (1967) for both swept and unswept leading edges. More recently, the unsteady nature of the interaction has been investigated by other researchers using more sophisticated measurement and analysis techniques. Schlieren photographs taken using a high speed camera with a framing rate of 35 kHz show that the centerline separation shock structure undergoes large variations and that the shock motion is random (Degrez 1981). The streamwise distance over which the shock foot translates is large scale (on the order of the fin thickness for unswept fins) and may vary from a fraction to several boundary layer thicknesses. Instantaneous wall pressure measurements have been made which generate detailed

information about the fluctuating load levels produced by the unsteady shock foot and root vortex (Dolling and Bogdonoff, 1981; Brusniak, 1991; Gonzalez and Dolling, 1993). A review of much of this material can be found in Dolling (1993). Computation of the flowfield has been attempted using a Baldwin Lomax turbulence model and full field Reynolds Averaged Navier Stokes calculations. The mean characteristics have been reproduced fairly accurately (Hung and Buning, 1985; Hung, 1989); however, computations do not predict the unsteadiness.

Experiments in which centerline properties were measured upstream of circular cylinders and hemicylindrically blunted fins show that the cylinder wake does not influence the upstream flowfield (Dolling, 1993). There can also be defined a fin height beyond which further increases in height do not change the centerline upstream influence and separation distance. Dolling and Bogdonoff (1981) found that in supersonic flows hemicylindrical fins could be treated as "semi-infinite" when their height to thickness ratios (h/t) were greater than about 2.4. All of the tests in this study and in studies used for comparison have been performed with semi-infinite fins in order to eliminate the additional complexity of a variation in results due to varying fin heights.

2.2 General Characteristics

2.2.1 Flow Structure and Length Scales

Using the evidence provided by many researchers the general flowfield structure can be described as follows. Separation of the boundary layer is caused by the strong adverse pressure gradient imposed by the fin bow shock. The separation itself produces a "separation shock". The intersection of the separation

shock and the bow shock is termed the triple point, and the overall root shock structure is called the λ -foot, because of its characteristic shape (Figure 1.1). Dolling and Bogdonoff (1982), among others, obtained mean surface streamline patterns using the kerosene-lampblack method flow visualization from which they deduced pertinent length scales of unswept fin-induced interactions. Typically the separation line, 'S', is visible in surface streamline visualization; in hemicylindrically blunted fin interactions, 'S' is 2-3t upstream of the fin leading edge. In all blunt fin-induced interactions, regardless of fin leading edge shape, 'S' is further upstream of and has a different curvature than the inviscid bow shock (Dolling and Rodi, 1988). From analysis of conditionally sampled fluctuating wall pressures Gramann and Dolling (1988) determined that the separation line visible in surface streamline flow visualization is actually the downstream boundary of a region of intermittent separation. Thus 'S' is the downstream boundary of the separation shock travel.

For semi-infinite fins the distance along the centerline from the fin leading edge to the separation line, L_{sep} , and upstream influence line, L_{ui} , are a function of fin thickness and leading edge geometry (Dolling and Rodi, 1988). For a fixed geometry they are only weakly dependent on Mach number and Reynolds number (Westkaemper, 1968). Measurements by Rodi at Mach 5 (Dolling and Rodi, 1988) show that for unswept fins with wedge shaped leading edges with half angles of 30° and larger, the upstream influence and separated flow lengths increase linearly with wedge angle, from 0.5 fin thicknesses at 30° to 6 fin thicknesses at 90° . Rodi also developed a correlation between fin leading edge drag coefficient, C_D , and separated flow length scale, L_{sep} . Thus, unswept fins with either hemicylindrical

or 53° half angle wedge leading edges, the configurations used in this study, each have $C_D \approx 1.0$, generate interactions with $L_{uj} \approx 2.8t$, and $L_{sep} \approx 2.4t$ (Dolling and Rodi, 1988).

2.2.2 Mean and RMS pressure Distributions

Figure 2.1 taken from Dolling (1993) shows distributions of mean pressure, $\overline{P_w}$, and RMS of pressure fluctuations, σ_{p_w} , on centerline upstream of hemicylindrically blunted fins at Mach 3 and Mach 5. The initial mean pressure rise at $X/t = -2.8$ defines the upstream influence of the interaction. It is typical for the mean pressure distribution to have two peaks (labeled P_M and P_{max} in Figure 2.1) and for the RMS distribution to have 3 peaks (labeled P_{R1} , P_{R2} , P_{R3}). Using measured pressure distributions similar to these and surface oil streak patterns, Robertson (1969) proposed a model for the flowfield ahead of the cylinder in which the boundary layer separates after being processed by the shock and forms a system of horseshoe vortices. A qualitative depiction of this system of vortices is shown in Figure 1.1. According to Robertson's model P_{R2} lies between the two major vortices.

The magnitude of the mean and RMS pressure levels depends on the fin thickness, t , and the incoming boundary layer thickness, δ . The effect of changes in each parameter may be combined in the ratio t/δ (Dolling and Bogdonoff, 1981). Increasing t/δ increases both the mean pressure (P_M in Figure 2.1) and the RMS pressure, (P_{R1} in Figure 2.1). This is explained by the fact that for larger t/δ "a greater fraction of the wave structure ahead of the fin root is effectively outside the boundary layer" (Dolling and Bogdonoff, 1981). In fact, as t/δ increases, P_M and

P_{R1} reach constant values. If more of the shock wave structure is immersed in the boundary layer, i.e. t/d decreases, the pressure rise due to the separation shock is attenuated and the structure itself is more dispersed, "consisting of a series of waves, rather than a single stronger shock" (Dolling and Bogdonoff, 1981).

2.2.3 Effect of Leading Edge Sweep

One of the earliest and most comprehensive investigations of swept fin-induced turbulent boundary layer separation was conducted by Price and Stallings (1967). The measurements included mean pressures and shadowgraph photography for sweep angles from 0° - 75° , Mach numbers from 2.3-4.44, and Re/m from 4.9×10^6 to 14.7×10^6 . This study showed that for hemicylindrically blunted fins increasing the leading edge sweep from 0° - 30° sharply decreases L_s , L_{ui} , and root pressure levels, P_{max} ; however, sweep has only a slight effect on the magnitude of P_M . This is because the pressure rise necessary to separate a particular boundary layer is essentially the same regardless of the geometry which generates the separation shock. For leading edge sweep angles above 30° the peak P_M was not resolved, and for sweep angles over 75° the effect of the model was "barely perceptible".

More recently Hussain (1985) obtained highly resolved static pressure distributions and detailed surface streamline patterns upstream of hemicylindrically blunted fins with sweep angles from 30° - 75° , Re/m of 2.95×10^6 , and Mach 2.4. Hussain confirmed that there was separated flow upstream of fins with sweep angles greater than 45° , which had not been directly observed previously. Better spatial resolution allowed the detection of the local pressure maximum, P_M , for

sweep angles up to 45°, but none was detected for greater sweep angles. Flowfield length scales in swept fin interactions, as in the case of unswept interactions, were found to scale, to first order, on fin leading edge thickness; however, there was considerable scatter. The best fit to the data as a function of leading edge sweep is given in the form

$$\frac{L_{sep}}{t} = 2.5 - 4.072\lambda + 2.513\lambda^2 - 0.605\lambda^3 \quad (2.1)$$

where t and λ are fin leading edge thickness and sweep angle respectively.

2.2.4 Application of Computational Fluid Dynamics

The general characteristics of unswept blunt fin-induced shockwave turbulent boundary layer interaction are reasonably well reproduced by CFD (Hung and Buning 1985; Hung, 1989). Calculations of the mean pressure distribution upstream of the fin are in good agreement with measurements, as shown in Figure 2.2. The local maxima/minima locations are reproduced as well as their magnitudes. Though the location of the maximum leading edge pressure is reproduced, its magnitude is slightly underpredicted. More important, though, is the fact that none of the unsteady aspects of the interaction are modeled in the numerical solutions of these flows, and thus fluctuating load levels can only be obtained from experiment.

2.3 Mean Flow Field Structure

Surface oil flow visualization, surface pressure distributions, and flowfield pitot pressure measurements have been used to infer the mean flow field structure

of blunt fin-induced shock wave turbulent boundary layer interactions (Voitenko, Zubkov, and Panov, 1966; Panov, 1966; Voitenko, Zubkov, and Panov, 1967). The result as depicted by Avduevskii and Medvedev (1967) is shown in Figure 2.3. Shock "1" is the bow shock; shock "2" is the instantaneous separation shock. A supersonic jet impinges on the surface of the fin/cylinder causing high pressures and forcing some quantity of freestream fluid to enter the separation zone. Figure 2.4(a-b) (Hung and Buning, 1985; Hung 1989) show full field Reynolds Averaged Navier Stokes calculations, using the Baldwin-Lomax turbulence model, of the particle paths on centerline upstream of a hemicylindrically blunted fin at Mach 3 and a flat faced fin at Mach 5 which show the recirculating nature of the separation vortex.

2.4 Unsteadiness of Shock Wave Turbulent Boundary Layer Interactions

2.4.1 General

It must be emphasized that the flowfield structure described above is true only in a time-averaged sense. The flowfield is unsteady and exhibits random changes in size and structure. Compared to the large eddy frequency of the incoming turbulent boundary layer (U_∞/δ), the frequency of the unsteady shock, as seen in power spectra of fluctuating pressures, is broadband and low, typically in the range 200 Hz - 2 kHz. The unsteady nature of the interaction has been observed qualitatively using spark schlieren and shadowgraph high speed photography (Degrez, 1981) and more recently quantitatively using fluctuating wall pressure measurements (Dolling and Bogdonoff, 1981; Brusniak and Dolling, 1991; Gonzalez and Dolling, 1993), fluctuating heat transfer measurements (Shifen and

Qingquan, 1990), and fluctuating mass flux measurements (Erengil, 1993). Analysis techniques developed at the University of Texas at Austin make it possible to extract quantitative data concerning the position and velocity of the separation shock foot from fluctuating wall pressure measurements. The algorithms used to perform these calculations are described briefly in Chapter 4.

As stated in section 2.2.1, the region between the upstream influence line and the separation line is characterized by an intermittent wall pressure signal. Figures 2.5-2.7 show typical pressure-time histories, probability density distributions, and power spectral density distributions. The signal in Figure 2.5(a) is from a transducer positioned upstream of the interaction. As expected, the signal is characterized by high frequencies. Figure 2.5(b) is from a point in the intermittent region. The pressures in the intermittent region exhibit high frequency, low amplitude fluctuations, superimposed on which are low frequency, high amplitude fluctuations. In this case, the transducer is under the undisturbed boundary layer for the majority of the time; however, for a fraction of the time the separation shock travels far enough upstream that it passes over the transducer, causing the low frequency pulses. This is borne out by the probability density distribution (Figure 2.6(b)) which is positively skewed since the most probable value of the signal, the undisturbed boundary layer pressure, is lower than the mean. The power spectral density distribution (Figure 2.7(2)) is dominated by the low frequency fluctuations caused by the translating shock.

Some observations of the unsteady nature of the interaction produced by *swept* fins in a Mach 2.5 flow have been made by Blank (1993) from schlieren movies with a framing rate of 4 kHz. For a 45° swept hemicylindrically blunted fin

he notes that "the separation shock is located roughly 0.5t upstream of the fin root and the areas affected by the unsteady separation shock are reduced with respect to the unswept case." In another experiment also carried out by Blank, the bases of the unswept and swept models were filleted with "skirts" (Figure 2.8) in an attempt to control or reduce the unsteadiness of the interaction. The result, however, was an increase in L_{ui} and L_{sep} and no reduction in the separation shock unsteadiness (Blank 1993). Further study using a fillet which was not thicker than the fin (Figure 3.3) produced "significant reduction of flowfield unsteadiness" (Blank 1993). To the author's knowledge, there are no quantitative data available in the literature concerning the effect of sweep or leading edge shape on separation shock dynamics.

The separated region of the interaction is comprised of counter-rotating horseshoe vortices. The number of vortices appears to be largely a function of Reynolds number. Fluctuating wall pressures in the separated region upstream of unswept cylinders and hemicylindrically blunted fins have been measured by Brusniak (1991) and Gonzalez and Dolling (1993). Wall pressures in this region are characterized by high amplitude, high frequency fluctuations. Mean pressure and fluctuating load levels at the fin root can be extremely high ($P_w/P_x \approx 9$, $\sigma_{P_w}/P_x \approx 3.5$). In contrast to the large eddy frequency of the incoming turbulent boundary layer ($U_\infty/\delta \approx 50$ kHz) the spectral content of pressure signals in the separated region is broadband with energy concentrated at approximately 25 kHz (Figure 2.7(6-7)). At this time little work has been done to quantify the unsteadiness of the separated region, and it is clear that more work is needed to determine the overall load levels, appropriate parameters for correlating power

spectra, and the nature of the mechanisms driving the low frequency separation shock motion.

2.4.2 Quantification of the Unsteadiness

A conditional sampling algorithm developed by Dolling and Brusniak (1989) extracts the low frequency high amplitude pressure fluctuations due to the separation shock from the high frequency low amplitude pressure fluctuations due to the turbulent boundary layer and separated flow. The algorithm permits consistent estimation of the time which the separation shock spends upstream and downstream of a particular transducer, as well as the precise times at which the shock passes over the transducer. Once it has been processed by the algorithm, the signal can be characterized quantitatively by the intermittency, γ , the fraction of time the separation shock is upstream of the transducer, and the zero-crossing frequency, f_c , the number of unidirectional crossings per second the separation shock makes over a particular position. The intermittency is normally distributed through the intermittent region, and $f_{c\max}$ occurs at 50% intermittency. The shock position, $X_s(t)$, and shock velocity, $V_s(t)$, can be determined if signals are acquired simultaneously from transducers spanning the intermittent region.

The fact that intermittency is normally distributed means that the shock has a "preferred position" in the center of the intermittent region, and that it spends equal time upstream and downstream of that position. Shock position histories show that the shock rarely makes low frequency periodic sweeps from 'S' to 'UI', but, rather, moves in a random manner. The shock motion is characterized by a low frequency random translation upstream and downstream superposed upon which is a high frequency jittering motion. The local maximum at low frequency in

the power spectral density distribution of pressure signals from the intermittent region is approximately the shock zero-crossing frequency at that point. It is not clear whether the length scales and frequency scales of the high frequency shock motion are adequately resolved with the current experimental setup since the transducers are a fixed distance ($\zeta=0.115$ in.) apart.

Gonsalez and Dolling (1993) show that to first order in a given boundary layer, the maximum zero-crossing frequency, which occurs at the center of the intermittent region (i.e. $\gamma=50\%$), is inversely proportional to intermittent region length (Figure 2.9). This is a result of the fact that the mean upstream and downstream shock velocities are constant regardless of the configuration producing the shock or the intermittent region length (Figure 2.10). Note that shock velocity calculations using data from small intermittent regions are slightly lower due to problems with the analysis technique, as discussed in section 4.2.2. Thus with constant shock velocity, as the region in which the shock traverses decreases in size, the number of crossings per second at the center of that region must increase. For a given incoming boundary layer, reducing the diameter of the fin, which reduces the intermittent region length, increases the shock zero-crossing frequency. The mechanism for this change in the shock dynamics is not clear, but it must be due in part to the downstream separated flow since the incoming conditions are fixed and only the fin thickness is altered.

2.4.3 Mechanisms of the Unsteadiness

The mechanisms driving the unsteady separation shock motion are not completely understood. Pressure fluctuations from the turbulent boundary layer

upstream of the separation shock and fluctuations from the separated flow region downstream of the separation shock each seem to play a role in setting the unsteady separation shock motion. Fluctuating wall pressure measurements in interactions with the same fin thickness but different incoming boundary layers, and then with the same incoming boundary layer but different fin thickness (Dolling and Smith, 1989) confirm this result (Figure 2.11). For interactions with the same incoming boundary layer, increasing the fin thickness increased the shock frequency. Likewise, for interactions with the same fin thickness and different boundary layers, decreasing the boundary layer thickness increased the shock frequency.

Gonsalez and Dolling (1993) show that for a given flowfield sweep angle power spectral density distributions in the intermittent region generated by different diameter fins (and thus with different intermittent region lengths) can be collapsed by plotting normalized power spectral density, $G(f) \cdot f / \sigma_p^2$, versus a Strouhal number, $f \cdot L_i / U_\infty$ (Figure 2.12). Dolling (1993) points out that although the scaling using L_i has a firm foundation, the validity of using U_∞ is not clear since all of the experiments were carried out at the same U_∞ . It bears repeating that changes in the spectra and in the intermittent region length can only have resulted from changes in the separated flow downstream of the separation shock, since the upstream conditions were identical in every case.

Brusniak (1991) investigated the role of fluctuations from the incoming boundary layer and from the separated region in driving the shock motion. Through ensemble averaging he showed that upstream propagation of large pressure pulses from the separated region into the intermittent region appeared to occur prior to changes in direction of the shock motion. The timing sequence of these events is

not entirely clear, but cross-correlations between pressure fluctuations at the downstream end of the intermittent region and successive positions downstream of it "showed large negative peaks at progressively more negative times, suggesting downstream to upstream propagation," (Brusniak, 1991). Erenkil (1991,2) and McClure (1992) used similar techniques to show that certain pressure "signatures" were visible in ensemble averages of the undisturbed boundary layer pressure-time histories for upstream and downstream shock sweeps. Thus specific types of fluctuation in the incoming boundary layer correlate with specific motions of the shock. Figures 2.13(a-b) show ensemble averaged wall pressure histories which were recorded only when the separation shock performed an upstream or downstream sweep respectively. The distinctive wall pressure signature, labeled 'sig', is different depending on whether the sweep is upstream or downstream, i.e. fall-rise-fall for upstream motion and rise-fall-rise for downstream motion. McClure points out that the pressure signature persists after being processed by the shock, thus turbulent structures remain coherent through the separation shock. From cross-correlations of pressure fluctuations in the incoming boundary layer and in the separated region Kleifges and Dolling (1992) showed that some fluctuations in the boundary layer affected the shock as they passed through it, and again affected it after being processed by the recirculation vortex.

In the current model proposed by Erenkil (1993) the motion of the shock is driven by the instantaneous static pressure ratio upstream and downstream of the shock. Fluctuations which change this ratio can occur either upstream of the separation shock (i.e. pressure fluctuations in the incoming boundary layer) or downstream of the shock from fluctuations in the separated region. As stated

before, there are two characteristic types of shock motion: a high frequency jitter, and a low frequency translation of the shock from 'S' to 'UI'. The current model proposes that the high frequency motions of the shock are due to fluctuations, both upstream and downstream of the shock, which originate in the incoming boundary layer. The low frequency motion of the shock seems to be influenced predominantly by fluctuations downstream of the shock, since this motion can be influenced by changes in fin geometry without changing the incoming boundary layer.

2.5 Summary

In the discussion above it appears that in blunt fin interactions both the upstream and downstream flowfields play a role in controlling the separation shock unsteadiness. This observation is the motivation of the current study in which the effects of leading edge sweep, leading edge shape, and fin root modifications on the flowfield unsteadiness is being investigated. In particular, an attempt is made to determine if differences in the separated region dynamics caused by leading edge changes cause the observed differences in separation shock dynamics.

CHAPTER 3

EXPERIMENTAL PROGRAM

3.1 Wind Tunnel

All experiments were conducted in the Mach 5 blow-down wind tunnel of the University of Texas at Austin. The test section is 6 inches wide by 7 inches high and is 27 inches long. Atmospheric air is compressed by a Worthington 4-stage compressor and stored at 2500 psig in several tanks with a combined volume of 4m³. The air is heated by two 420 kW banks of nichrome wire heaters before it enters the tunnel stagnation chamber. The maximum run time is about 60 seconds. All tests were conducted under the conditions stated in Table 3.1.

Table 3.1: Freestream Flow Conditions

M_∞	4.95
P_0	333 psia
P_∞	0.617 psia
T_0	620°R
V_∞	2500 ft/sec
Re	$14.9 \times 10^6 \text{ ft}^{-1}$

The incoming boundary layer underwent natural transition in the nozzle far upstream of the test section. Measured boundary layer properties are given in Table 3.2.

Table 3.2: Boundary Layer Properties (McClure, 1991).

δ_0	0.59 in.	$H \equiv \delta^*/\theta$	10.2
δ^*	0.26 in.	Re_θ	3.16×10^4
θ	0.026 in.	C_f	7.74×10^{-4}
Π	0.78		

3.2 Experimental Methods

3.2.1 Surface Tracer Flow Visualization Method

A mixture of carbon lampblack, diesel fuel, and kerosene was used to obtain surface streamline patterns of the separated flowfield upstream of each model. The exact amount of each component of the mixture was determined by trial and error in order to get the best quality flow visualization results. A run time of 20 seconds was sufficient to dry the kerosene and diesel, and then the carbon lampblack powder could be removed from the tunnel floor on a large sheet of transparent tape with the surface streamline pattern intact. This method allows accurate measurements of flow field length scales, since measurements are made directly from an undistorted image. However, the method has zero frequency response, and thus the pattern provides no information about the dynamic aspects of the interaction.

3.2.2 Fluctuating Wall Pressure Measurement

Miniature Kulite pressure transducers (model XCQ-062-50A) were used to measure instantaneous wall pressure. These transducers have a nominal outer diameter of 0.0625 inches and were mounted flush with the tunnel floor. The

frequency response is limited to approximately 50 kHz due to a protective screen above the 0.028 inch diameter silicon diaphragm. Full scale output is nominally 75 mV for an applied pressure of 50 psia, resulting in a sensitivity of 1.5 mV/psi. The combined nonlinearity and hysteresis are given by the manufacturer as 0.5% BFSL (Best Fit Straight Line), and the maximum change of sensitivity with temperature is 8%/100°F for an operating range of -65°F to 250°F. Repeatability is 0.1% FS (Manufacturer's Specification).

The signals from the transducers were amplified by either PARC (Model 113) or Dynamics (Model 7525) amplifiers and low-pass filtered by an Ithaco (Model 4113 or Model 4213) electronic filter. Amplifier gains were set during calibration before each run to maximize transducer output, thus gain varied depending on the expected pressure range. The filters were set at 50 kHz (lowpass mode) due to the 50 kHz frequency response of the transducers. For the runs made at 100 kHz sampling frequency the filters were set at 40 kHz to avoid aliasing.

After amplification and filtering, the transducer signals were digitized by two LeCroy 6810 waveform recorders equipped with 12-bit A/D converters. All tests were performed using the 0-4 V unipolar mode. The data were stored and processed using a Hewlett Packard HP 9000 workstation. In a typical test using 8 transducers, 512 records of data per channel with 1024 samples per record were acquired.

In each run eight transducers were placed in a row on the fin centerline upstream of the model. The center to center spacing between adjacent transducers, ζ , was 0.115 inches. In subsequent runs the transducers were moved further upstream so that data could be obtained from the fin root through the entire

interaction. Furthermore, to increase spatial resolution, runs were made with the model shifted by 0.5ζ with the same transducer layout.

3.3 Models

In order to study the effect of leading edge sweep on separation shock dynamics, five 0.75 inch thick hemicylindrically blunted fins with leading edge sweep angles, λ , of 0° , 8° , 18° , 30° , and 45° were used (Figure 3.1). Previous studies by Price and Stallings (1967) and Hussain (1985) show that sweep reduces L_{ui} , but do not provide any information on how the unsteady aspects of the interaction are affected.

It was observed by Rodi and Dolling (1988) that more than one leading edge shape could produce an interaction with a particular upstream influence. However, upstream influence is a characteristic of the mean interaction, and the dynamics of the separation shock in different flows with the same upstream influence might be significantly different. Useful information about the driving mechanism of these interactions could be obtained if a conclusion can be made about whether the differences in separation shock dynamics are explained by differences in separated region dynamics. To pursue this question, pressure measurements were made on centerline in three interactions with essentially the same upstream influence. Two 0.75 inch thick unswept fins, one with a hemicylindrically blunted leading edge and one with a 53° half angle wedge shape leading edge, and a 0.375 inch thick flat-faced fin were used because they each produce an interaction with approximately the same centerline upstream influence.

The choice of 0.375 inches for the thickness of the flat-faced fin was based on the results of Rodi and Dolling (1988). However, since different methods were used to estimate upstream influence in the present study and that of Rodi and Dolling, the earlier measurements could not be used directly. The value of upstream influence for the hemicylindrically blunted fin defined by 1% intermittency is $3.5t$, whereas using mean pressure measurements as was done by Rodi and Dolling it is $2.75t$. It was assumed that the same difference in prediction would apply to the flat-faced fin and the predicted upstream influence was scaled by $3.5/2.75$ resulting in $7t$ instead of $5.5t$ as predicted by Rodi and Dolling. The dimensions of the wedge-shaped and flat-faced fins are shown in Figure 3.1-3.2. The height to thickness ratio of every fin used in these experiments was greater than 5 and thus each can be considered semi-infinite (Dolling and Bogdonoff, 1981).

Preliminary results from the swept fin interactions showed significant reductions in L_{ui} and L_i with increasing leading edge sweep, consistent with earlier work of Price and Stallings (1967) and Hussain (1985). To examine whether the same effect could be obtained using a minor modification to the unswept fin root rather than sweeping the entire fin leading edge, a 45° swept fillet was attached to the leading edge root of the unswept fin (Figure 3.3). High speed schlieren photography made by Blank (1993) suggested that this type of fillet reduced the unsteadiness, and thus this experiment was a quantitative test of that observation. Preliminary results from the fillet tests indicated a considerable reduction in the size of the interaction and its unsteadiness. Thus a second modification was made to the unswept hemicylindrically blunted fin in the form of a swept strake, similar to the

swept fillet except that it was only 0.060 inches thick (Figure 3.4). The purpose of this configuration was to determine if the same reduction in the interaction unsteadiness could be attained using a simpler geometry.

3.4 Test Program

Recall that the objectives of this research are: (i) determine the effect of leading edge sweep and leading edge shape on the fluctuating loads and shock dynamics; (ii) determine the feasibility of using minor fin root modifications to favorably influence the unsteadiness of the interaction; and (iii) determine if differences in the separated region dynamics caused by leading edge changes cause the observed differences in separation shock dynamics.

To meet these objectives two types of data sets were collected using each of the models: (1) fluctuating wall pressures were measured along the centerline of the entire interaction using eight transducers at a time; (2) fluctuating wall pressures were measured simultaneously upstream of the interaction, in the intermittent region, and in the separated region. The first data set was used to determine the effects of leading edge sweep, leading edge shape, and fin root modifications on the separation shock dynamics and the dynamics of the separated region. The second data set was collected to allow cross-correlations between transducers upstream and downstream of separation in order to determine, if possible, cause and effect.

CHAPTER 4

ANALYSIS TECHNIQUES

4.1 General Time Series and Statistical Analysis

The results in this thesis were obtained by applying basic statistical analysis, standard time-series analysis, and conditional sampling algorithms to the fluctuating pressure signals. Statistical analysis consisted of calculations of the mean, standard deviation, skewness and flatness coefficients and the amplitude probability density distribution of each pressure signal. Time-series analysis consisted of cross-correlations, auto correlations, and power spectral density estimates. Details of the calculation of these quantities are given by Bendat and Piersol (1986).

4.2 Conditional Sampling

4.2.1 Shock Statistics Algorithm

A conditional sampling algorithm was used to convert the intermittent wall pressure-time histories into digital boxcar signals which could be analyzed to quantify the separation shock statistics. The algorithm was first developed by Narlo (1986) and later refined by Brusniak (1988) and Dolling and Brusniak (1989). The purpose of the algorithm is to distinguish the rises and falls in pressure due to the passage of the separation shock from those due to turbulent fluctuations in the undisturbed and separated boundary layer.

The algorithm first determines the mean and RMS pressure of the undisturbed boundary layer portion of the signal, \bar{P}_{w0} and $\sigma_{p_{w0}}$, respectively. Using these values two thresholds are defined: $T_1 = \bar{P}_{w0} + 3\sigma_{p_{w0}}$ and $T_2 =$

$\bar{P}_{w0} + 6\sigma_{p_{w0}}$. Sensitivity analysis (Brusniak, 1988; Dolling and Brusniak, 1989) showed that this formulation of the thresholds yielded "physically meaningful results". Using these thresholds the algorithm searches through the data set and determines the rise- and fall-time associated with each shock passage. As illustrated in Figure 4.1, when the pressure rises above T_2 a rise-time, t_r , is recorded, and when the pressure then falls below T_1 a fall-time, t_f , is recorded. Using this information the shock zero-crossing frequency, f_c , and intermittency, γ , defined by

$$f_c = \frac{1}{\frac{1}{N} \sum_{i=1}^{N-1} (t_{r,i+1} - t_{r,i})} \quad (4.1)$$

$$\gamma = \frac{\sum_{i=1}^N (t_r - t_f)_i}{t_{total}} \quad (4.2)$$

where N is the number of shocks detected, are calculated. The zero crossing frequency is the number of unidirectional crossings per second, and thus is a measure of how often the shock passes over a given location in the intermittent region. The intermittency is the fraction of the total time that the shock is upstream of a particular location.

The rise- and fall-times can also be recorded as a digital boxcar signal. For time $t_r < t < t_f$ the boxcar signal is given the value '1', and for all other times the signal is given the value '0'. Boxcar signals derived in this manner are used by other algorithms described below to quantify the dynamics of the separation shock motion.

4.2.2 Separation Shock Foot Position and Velocity Histories

Although it is difficult to measure directly the position of the separation shock foot, it is possible to bracket its location from multi-channel surface pressure fluctuations (Erengil, 1992). The times at which the shock crosses each transducer are discretized by the conditional sampling algorithm described above. The binary boxcar signals can be nested and the shock position deduced as being either upstream of the transducer array, downstream of the array, or between two adjacent transducers.

Figure 4.2(a) (Erengil, 1992) shows an example set of transducers. Nested boxcar signals from compression ramp data are shown in Figure 4.2(b). The rise- and fall-times in the boxcar signals identify the coordinates of the instantaneous position of the shock foot. The position of the shock foot can be estimated for any intermediate time by linear interpolation of these coordinates, and the result is a piece-wise smooth function for the shock position, $X_s(t)$ as shown in Figure 4.2(c). The separation shock velocity history, $V_s(t)$, can be calculated by differentiating $X_s(t)$, (Figure 4.2(d)). Once $X_s(t)$ and $V_s(t)$ have been obtained from the boxcar signals, standard time series analysis can be used to quantify the shock dynamics and these statistical characteristics can be compared from interaction to interaction.

The only assumptions made are that the shock moves in one direction at constant speed as it passes from one transducer to the next. In the case of the shock turning around, it is assumed to travel to the midpoint between two transducers, change direction, and move back at the same speed. Inspection of $X_s(t)$ and $V_s(t)$ in Figure 4.2(c-d) shows that the assumed velocities during shock turnarounds and for time which the shock spends in the upstream and downstream bins are not

radically different from those calculated from precise knowledge of the shock position. This is not the case, however, if the transducers whose signals are converted do not capture a large portion of the intermittent region. In such a case, the shock spends a disproportionate amount of time in the upstream or downstream bin, and the assumed velocity is not representative of the actual velocity, causing the shock velocity statistics to be skewed toward the assumed value. Gonzalez (1993) modified the code so that it ignores velocities calculated using the assumption that the shock travels at constant velocity while it resides in the far upstream or downstream bin.

4.2.3 Calculation of Interaction Length Scales

The distance to separation, L_{sep} was measured directly from flow visualization. The intermittent region length, L_i , was calculated using a curve fit of the error function, $y = \text{erf}(x)$, to the intermittency curves produced by the shock statistics algorithm. L_{ui} is taken as the distance from the fin leading edge to the location of 1% intermittency and L_i is taken as the distance between points with $\gamma = 5\%$ and 95% . The implicit assumption is that the intermittency is normally distributed between 'UI' and 'S', and experiments have shown this to be the case (Erengil and Dolling, 1991).

CHAPTER 5

RESULTS

5.1 Effects of Leading Edge Sweep

5.1.1 Mean and RMS Pressure Distributions

The mean pressure distributions for all of the hemicylindrically blunted fin cases (Figure 5.1(a)) show that increasing leading edge sweep is accompanied by a decrease in the distance to the first pressure peak, P_M , a slight decrease in the magnitude of P_M , and a considerable decrease in the mean pressure at the fin root, P_{max} . Figure 5.1(b-c) show the variation of magnitude of P_M and P_{max} with leading edge sweep angle. P_M is essentially constant with sweep angle, whereas in the range $0^\circ < \lambda < 30^\circ$ P_{max} decreases linearly. Beyond this range there is little or no change in P_{max} . Spatial resolution difficulties preclude detection of P_M for sweep angles greater than 30° . These results are consistent with the work of Price and Stallings (1967), up to 30° , and Hussain (1985), up to 45° .

The RMS pressure distributions (Figure 5.2(a)) show that the magnitudes of the local maxima P_{R1} and P_{R2} are the same and do not vary initially with increased sweep, then decrease for sweep angles greater than 18° (Figure 5.2(b)). The root RMS loading level decreases rapidly with increasing sweep, approximately linearly for sweep angles of 0° - 18° , and then less rapidly for greater sweep angles (Figure 5.2(c)).

Caution is needed in interpreting some of these data. Pressure measurements were not always made at the fin root itself, rather 0.5ζ upstream of the root. Thus the values of P_{max} and P_{R3} are the highest *measured* values, not

necessarily the absolute *maxima*. The mean and RMS pressure values for the 18°-45° cases suffer the most from poor spatial resolution due to small interaction size, and thus may be slightly underpredicted. Those values in the larger interactions were adequately resolved. Finally, the RMS data are more reliable than the mean pressure data since the RMS values are not susceptible to the systematic errors introduced by calibration drift, or to zero shift due to temperature changes.

5.1.2 Flow Length Scales

Figure 5.3(a-c) show the variation of overall interaction size, L_{ui} , intermittent region length, L_i , and separation length, L_{sep} , with leading edge sweep angle. There is a linear decrease in each for sweep angles of 0°-18°. Figure 5.3(d) shows that the intermittent region is, in fact, an ever increasing fraction of the total interaction length as sweep angle increases. If leading edge sweep was increased sufficiently the interaction would be dominated by the intermittent region, although its length scale would be very small. A similar observation has been made in compression corner experiments with very small corner angles where the shock strength is not great enough to cause separation but fluctuations in the turbulent boundary layer still cause small scale random motion of the corner shock (Dolling and Or, 1985). Thus the separation shock motion is affected directly by fluctuations in the incoming boundary layer as well as indirectly by the fin leading edge geometry.

5.1.3 Zero-Crossing Frequency and Power Spectral Density Distributions

The zero-crossing frequency, f_c , is the number of unidirectional crossings per second of the separation shock over a point in the intermittent region. Figure 5.4(a) shows the zero-crossing frequency distributions for each leading edge sweep angle. Figure 5.4(b) shows the variation of the maximum zero-crossing frequency, $f_{c,max}$ (which occurs at $\gamma=50\%$) with leading edge sweep. Although the RMS pressure levels at this position are the same for moderate leading edge sweep angles, $f_{c,max}$ increases as leading edge sweep angle increases. The weak trend of increasing $f_{c,max}$ for 8° and 18° is much more significant between 18° and 45° . This trend can be explained qualitatively through examination of the separation shock velocity histories. The mean shock velocity is constant regardless of sweep angle and intermittent region length. Thus, with a constant mean shock velocity but a smaller region in which to translate (as seen in Figure 5.4(c)), the shock frequency naturally increases.

Power spectral density distributions (PSDs) from the center of the intermittent region ($\gamma=50\%$) are shown in Figure 5.5(a-b) in dimensional and normalized forms respectively. For moderate sweep angles ($0 < \lambda_{LE} < 18$), where the RMS of the pressure fluctuations is the same, there is a slight decrease in low frequency energy content which is balanced by a corresponding increase in high frequency energy content. The 30° and 45° cases have a decrease in energy at low and high frequencies. The normalized spectra (Figure 5.5(b)) are presented because this representation is not biased by changes in variance among the various cases. The normalized spectra show that a large fraction of the overall variance of signals from the intermittent region is produced by low frequency fluctuations. The

maximum of each of the normalized spectral density curves occurs close to the maximum shock zero-crossing frequency, $f_{c_{max}}$, showing that pressure fluctuations due to the shock motion dominate the spectral content of pressure signals from the intermittent region.

Power spectra in the separated region are shown in Figure 5.6(a-b). The spectra are from different interactions but at points which are at the same relative position in the RMS pressure distribution ($\sigma_p/\overline{P_w} = 0.17$, downstream of 'S'). This position was chosen because the spectra in this region are not sensitive to small changes in streamwise location. The spectra are broadband in nature and a much greater portion of the variance comes from high frequencies than in signals from the intermittent region. The effect of increasing sweep is a slight increase in low frequency energy content and a corresponding decrease in high frequency content, but to first order the spectra are essentially identical.

Dimensional and normalized PSDs of pressure fluctuations at the fin root of each swept fin are shown in Figure 5.7(a-b). The decrease in RMS pressure at the fin root is responsible for the decrease in magnitude of the dimensional PSDs. The normalized PSD's show that accompanying the reduction in RMS there is redistribution of energy to higher frequencies; however, to first order, sweep has little effect on the spectral content of the fluctuating wall pressure signals.

5.1.4 Summary of Effects of Leading Edge Sweep

Despite the questions of spatial resolution, the results show the practical benefits to be obtained from leading edge sweep. Although the mean and RMS pressure loading levels in the intermittent region are unaffected by moderate

sweepback, the mean and RMS pressures at the fin root were reduced by 40% and 60% respectively with 18° of leading edge sweep. This reduction in root loading is coupled with a significant reduction of the interaction length scale (by 82% in the 45° case). Leading edge sweep has little effect on the spectral content of the pressure fluctuations in the separated region, but the spectral content of fluctuations in the intermittent region shifts to higher frequencies for greater sweep angles.

5.2 Effects of Changes in Leading Edge Shape

5.2.1 Mean and RMS Pressure Distributions

Figures 5.8(a-b) show the mean and RMS pressure distributions upstream of the three unswept fins with wedge-shaped, hemicylindrical, and flat-faced leading edges. As anticipated, the three interactions have approximately the same overall length scale. The magnitudes of P_M and P_{R1} are similar for each interaction. Also, the location of each of the maxima is slightly further from the fin root for the "blunter" configurations and, as would be expected, the "blunter" configurations produce higher mean and RMS loading levels at the fin root.

5.2.2 Flow Length Scales

Figures 5.9(a-c) show how L_{ui} , L_i , and L_{sep} vary with leading edge shape. As intended, each interaction has approximately the same L_{ui} . The "blunter" cases have smaller intermittent region lengths and correspondingly larger separated region lengths.

5.2.3 Power Spectral Density Distributions

The power spectral density distributions (PSDs) from the intermittent region of the three equivalent sized interactions are very similar (Figure 5.10(a-b)). The normalized form illustrates the same trend as spectra from the swept fin flows: the maximum is near the maximum zero crossing frequency. Spectra from the separated region are almost indistinguishable (Figure 5.11(a-b)). Likewise, though there is a significant shift in the dimensional PSDs at the fin root due to the change in RMS pressure, normalized PSDs show that there is little difference in the relative distribution of the variance in the frequency domain (Figure 5.12(a-b)).

5.2.4 Summary of the Effects of Leading Edge Shape

The results from these experiments show clearly that the shape of the fin leading edge can be used to alter the unsteadiness of the shockwave turbulent boundary layer interaction. Although the interactions produced by the different leading edges were identical in upstream extent, the root loading, the intermittent region loading, intermittent region length, and the separation distance varied depending on the bluntness of the leading edge. It is not yet clear how the changes observed in the interaction are influenced by the separated flow dynamics. Since the variation in the flow length scales is connected to the bluntness of the leading edge, it appears from a qualitative point of view that the variations are due to increased recirculation of turbulent structures which would occur upstream of the more blunt configurations.

5.3 Leading Edge Modifications

5.3.1 Filleted Fin Root

The 45° fillet had a profound effect on the flowfield upstream of the unswept hemicylindrically blunted fin. The flow visualizations from the modified and unmodified unswept fin are shown in Figure 5.13. At all spanwise locations the separation line from the filleted fin is well downstream of the separation line from the unmodified fin. However, the effect of the fillet modification is limited in spanwise extent, and the intersection between the fillet bow shock and the fin bow shock (marked '1' in Figure 5.13) should be investigated to determine whether loading levels are not higher in this new flowfield than in the unmodified flowfield.

Figures 5.14(a-b) show the centerline mean and RMS pressure distributions upstream of the unswept hemicylindrically blunted fin with and without the modification, and upstream of the 45° swept fin. The centerline distributions upstream of the 45° swept fin and the upstream of the 45° fillet are identical. Compared to the unswept case the upstream influence and the intermittent region lengths were reduced by 50%. The mean and RMS loading levels at the fin root are reduced by 75% and 45% respectively.

The use of the swept fillet fin root modification is an excellent way to obtain the benefits of leading edge sweep without sacrificing the surface area of a control surface.

5.3.2 Unswept Fin with Strake Modification

Flow visualization results from the unswept fin with strake modification showed that the interaction was unaffected by the leading edge modification. The

separation distance and the separation shock curvature were identical to the unmodified case, and hence no further tests were made.

5.4 Flow Physics

As noted in the introduction, an exploratory attempt has been made to detect differences in the separated regions of interactions with different shock dynamics. Although every configuration tested in these experiments exhibited the same characteristic mean and RMS pressure distributions, the shock dynamics, as described by the zero-crossing frequency and the power spectral density distributions from the intermittent region, were different in each case. If turbulent fluctuations are responsible for the shock dynamics, then differences in the shock dynamics must be caused by changes in the fluctuations in the separated region since the upstream conditions were identical for each case. However, the use of standard time-series analysis methods to detect the connection between changes in leading edge geometry, changes in the dynamics of the separated region and changes in separation shock dynamics has been elusive.

5.4.1 Cross-correlations of Signals from Adjacent Transducers

Cross correlations, which give information about the relative timing between events on two signals which are correlated, were used to attempt to determine differences in the dynamics of fluctuations in the various separated regions. Figure 5.15(a) shows a typical cross-correlation of two adjacent transducers in the separated region. Peak '1' shows a large positive correlation at

positive time delay, τ , indicating downstream flow of coherent turbulent structures. For a given transducer spacing, the timing of Peak '1' is independent of location within the separated flow and the time delay corresponds to a convection velocity of $0.75U_\infty$, which is slightly less than the convection velocity in the undisturbed boundary layer and is therefore consistent with deceleration through the shock wave. Thus, Peak '1' is due to turbulent structures in the separated shear layer passing over the transducer.

Peaks '2' and '3', which are not seen in cross-correlations of the undisturbed turbulent boundary layer shift symmetrically to greater positive and negative values of τ respectively as the transducer pair moves further downstream in the separated region. A satisfactory explanation of this trend is unclear; however, the phenomenon being observed appears to be the entrainment of turbulent structures from the separated shear layer. As the fluid is entrained and is forced down toward the wall, it moves either upstream or downstream, and this motion is reflected in the cross-correlations as Peaks '2' and '3'. This process is described qualitatively in figure 5.15(b).

Cross-correlations of adjacent transducers at the same relative location in the three interactions generated by different shaped leading edges is shown in Figure 5.16. The correlations are remarkably similar. The slight timing difference between peaks in the correlation upstream of the flat faced fin is most easily explained by sensitivity to location, not by differences in the flow. Thus the cross-correlations do not provide any evidence of significant differences between the three separated flows.

5.4.2 Correlation of Signals Upstream and Downstream of Separation

Cross-correlations were also calculated between signals under the undisturbed boundary layer and signals in the separated region, for the three identically sized interactions in order to see if any evidence could be found concerning differences in the recirculation of turbulent structures. Furthermore, differences in the recirculation in the different cases might be used to explain the mechanism driving the shock motion.

In order to correlate signals at the same relative position in the separated region, the distance between the two transducers is different in each case. Thus, the timing of the initial peak due to the passage of turbulent structures in the separated shear layer (Figure 5.17(a)) is different for each case. When the time delay for each case is normalized by the time for the freestream to travel between the two transducers the peaks align (Figure 5.17(b)). This primary peak is simply evidence of the convection of turbulent structures through the interaction. The secondary maxima in the cross-correlations are evidence of recirculation; however, the differences between the three cases are minor and thus the cross-correlations provide no obvious evidence of differences between the three flows. Clearly this is an area where more work using more sophisticated approaches is needed.

CHAPTER 6

CONCLUSIONS

Fluctuating wall pressure measurements have been made on centerline upstream of blunt fins in a Mach 5 flow. Standard time series analysis and conditional sampling algorithms have been used to examine the effects of leading edge sweep, leading edge shape, and fin root modifications on the unsteadiness. The results show that fluctuating loads can be reduced by appropriate modification of the fin leading edge.

- (1) Leading edge sweep considerably reduced the mean and RMS pressure loading at the fin root, the intermittent region length, and the separation length. The spectral content of pressure fluctuations in the intermittent region was concentrated at the shock zero-crossing frequency for each case, while the spectral content of pressure fluctuations in the separated region was virtually unchanged by leading edge sweep.
- (2) Geometries which induce the same size interaction with different leading edge shapes were found to have different intermittent and separated region lengths depending on the bluntness of the leading edge shape. The more blunt configurations produced smaller intermittent regions and larger separated regions.
- (3) While the use of the strake as a modification to the unswept fin was found to have no effect, the fillet modification reduced the centerline upstream influence and intermittent region length by 50%, and reduced the mean and RMS pressure loading at the fin root by 75% and 95% respectively.

- (4) At this time it is not possible to make a conclusion about whether differences in the separated region dynamics are responsible for the observed changes in the shock dynamics in the intermittent regions of the various configurations tested. Further analysis of these data using different analysis techniques might make this possible.

REFERENCES

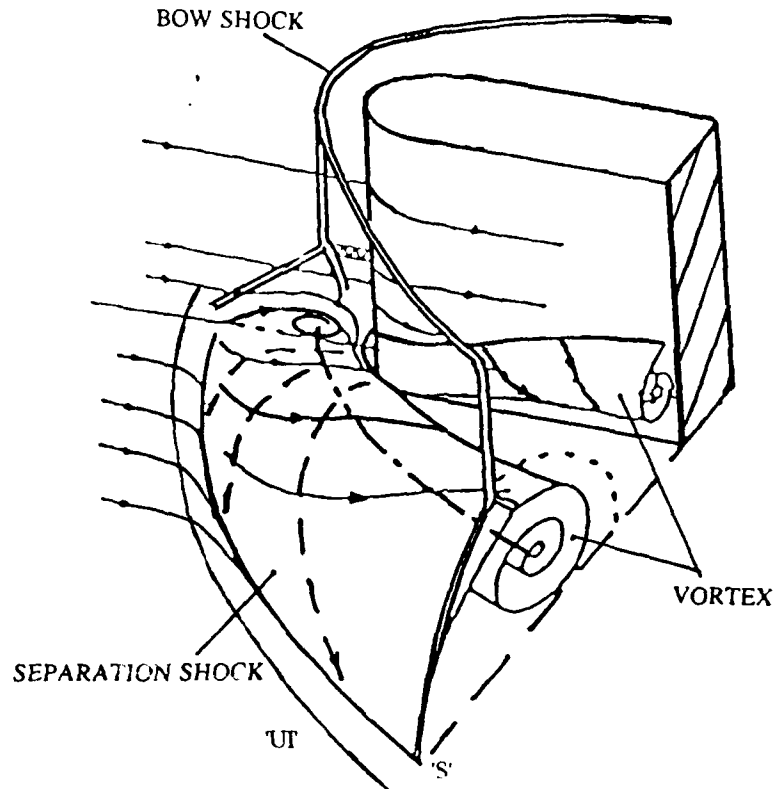
- [1] Avduevskii, V.S., and Medvedev, K.I. (1967), "Physical Properties of the Flow in the Separation Region for Three-Dimensional Interactions of a Boundary Layer with a Shock Wave," *Akademiya Nauk SSSR, Izvestiya, Mekhanika Zhidkosti i Gaza*, Vol. 2, No. 1, pp. 25-33, 1967; trans. in the Johns Hopkins University Applied Physics Laboratory Library Bulletin.
- [2] Bendat, J.S., and Piersol (1986), A.G., Random Data, Analysis and Measurement Procedures, 2nd Ed., John Wiley & Sons, New York, 1986.
- [3] Blank, S.C. (1992,1993), "The Effect of Junction Modifications on Glancing Interaction--Blunt Fins," Private Communication, January 1993.
- [4] Brusniak, L. (1988), "Evaluation of Conditional Sampling Methods of Analyzing Separation Shock Motion," AIAA Paper 88-0091, 26th Aerospace Sciences Meeting, Reno, Nevada, January 1988.
- [5] Brusniak, L. (1991), "Experimental Investigation of the Driving Mechanism of the Unsteady Separation Shock Motion in a Cylinder-Induced Hypersonic Interaction," M.S. Thesis, Department of Aerospace Engineering and Engineering Mechanics, University of Texas at Austin, May 1991.
- [6] Brusniak, L. (1993), Private Communication, February 1993.
- [7] Degrez, G. (1981), "Exploratory Experimental Investigation of the Unsteady Aspects of Blunt Fin-Induced Shock Wave Turbulent Boundary Layer Interactions," M.S.E. Thesis 1516-T, Mechanical and Aerospace Engineering Department, Princeton University, Princeton, NJ, June 1981.
- [8] Dolling, D.S. (1993), "Fluctuating Loads in Shock Wave/Turbulent Boundary Layer Interaction: Tutorial and Update," AIAA Paper 93-0284, 31st Aerospace Sciences Meeting & Exhibit, Reno, Nevada, January 1993.
- [9] Dolling, D.S., and Bogdonoff, S.M. (1981), "An Experimental Investigation of the Unsteady Behavior of Blunt Fin-Induced Shock Wave Turbulent Boundary Layer Interactions," AIAA Paper 81-1287, 14th Fluid and Plasma Dynamics Conference, Palo Alto, California, June 1981.

- [10] Dolling, D.S., and Bogdonoff, S.M. (1982), "Blunt Fin-induced Shockwave Turbulent Boundary Layer Interaction," *AIAA Journal*, Vol. 20, No. 12, December 1982, pp. 1674-1680.
- [11] Dolling, D.S., and Brusniak, L. (1989), "Separation Shock Motion in Fin, Cylinder, and Compression Ramp-Induced Turbulent Interactions," *AIAA Journal*, Vol. 27, No. 6, pp. 734-742, June 1989.
- [12] Dolling, D.S., and Or, C.T. (1985), "Unsteadiness of the Shock Wave Structure in Attached and Separated Compression Ramp Flows," *Experiments in Fluids*, Vol. 3., pp. 24-32, 1985.
- [13] Dolling, D.S., and Rodi, P.E. (1988), "Upstream Influence and Separation Scales in Fin-Induced Shock Turbulent Boundary Layer Interaction," *Journal of Spacecraft and Rockets*, Vol. 25, No. 2, pp. 102-108, March-April 1988.
- [14] Dolling, D.S. and Smith, D.R. (1989), "Separation Shock Dynamics in Mach 5 Turbulent Interactions Induced by Cylinders," *AIAA Journal*, Vol. 27, No. 12, pp. 734-742, June 1989.
- [15] Erengil, M.E. (1993), Private Communication, February 1993.
- [16] Erengil, M.E. and Dolling D.S. (1991), "Correlation of Separation Shock Motion with Pressure Fluctuations in the Incoming Boundary Layer," *AIAA Journal*, Vol. 29, No. 11, pp. 1868-1877, November 1991.
- [17] Erengil, M.E., and Dolling, D.S. (1992), "Effects of Sweepback on Unsteady Separation in Mach 5 Compression Ramp Interactions," AIAA Paper 92-0430, 30th Aerospace Sciences Meeting, Reno, Nevada, January 1992.
- [18] Gonzalez, J.C., and Dolling, D.S. (1993), "Correlation of Interaction Sweepback Effects on the Dynamics of Shock-Induced Turbulent Separation," AIAA Paper 93-0776, 31st Aerospace Sciences Meeting and Exhibit, Reno, Nevada, January 1993.
- [18] Gonzalez, J.C. (1993), Private Communication, February 1993.
- [19] Hung, C-M. (1989), "Computation of Navier-Stokes Equations for Three-Dimensional Flow Separation," NASA TM 102266, December 1989.

- [20] Hung, C-M., and Buning, P.G. (1985), "Simulation of Blunt Fin Induced Shock Wave and Turbulent Boundary Layer Interaction," *Journal of Fluid Mechanics*, Vol. 154, pp. 163-185, May 1985.
- [21] Hussain, S. (1985), "A Study of the Interaction Between a Glancing Shock Wave and a Turbulent Boundary Layer--The Effects of Leading Edge Bluntness and Sweep," Ph.D. Thesis, College of Aeronautics, Cranfield Institute of Technology, November 1985.
- [22] Kleifges, K. and Dolling, D.S. (1992) "Control of Unsteady Shock-Induced Turbulent Boundary Layer Separation Upstream of Blunt Fins," Abstract submitted for presentation at AIAA 3rd Annual Shear Flow Control Conference, July 1993. Copies available from second author.
- [23] McClure, W.B. (1991), Unpublished boundary layer properties for Balcones Research Center Mach 5 Wind Tunnel, The University of Texas at Austin, October 1991.
- [24] McClure, W.B. (1992), "An Experimental Study of the Driving Mechanism and Control of the Unsteady Shock-Induced Turbulent Separation in a Mach 5 Compression Corner Flow," Ph.D. Dissertation, Dept. of Aerospace Engineering and Engineering Mechanics, The University of Texas at Austin, August 1992.
- [25] Narlo, J.C. (1986), "Experimental Investigation of the Driving Mechanisms of Separation Shock Wave Motion in Interactive Flows," M.S. Thesis, Department of Aerospace Engineering and Engineering Mechanics, University of Texas at Austin, December 1986.
- [26] Panov, Y.A. (1966), "Interaction of a Three-Dimensional Shock Wave with a Turbulent Boundary Layer," *Akademiya Nauk SSSR, Izvestiya, Mekhanika Zhidkosti i Gaza*, Vol. 1, No. 4, pp. 185-188, 1966; trans. in the Johns Hopkins University Applied Physics Laboratory Library Bulletin.
- [27] Price, E.A., and Stallings, R.L. (1967), "Investigation of Turbulent Separated Flows in the Vicinity of Fin-Type Protuberances at Supersonic Mach Numbers," NASA TN D-3804.
- [28] Settles, G.S., and Dolling, D.S. (1990), "Swept Shock/Boundary Layer Interactions: Tutorial and Update," AIAA Paper 90-0375, 28th Aerospace Sciences Meeting, Reno, Nevada, January 1990.

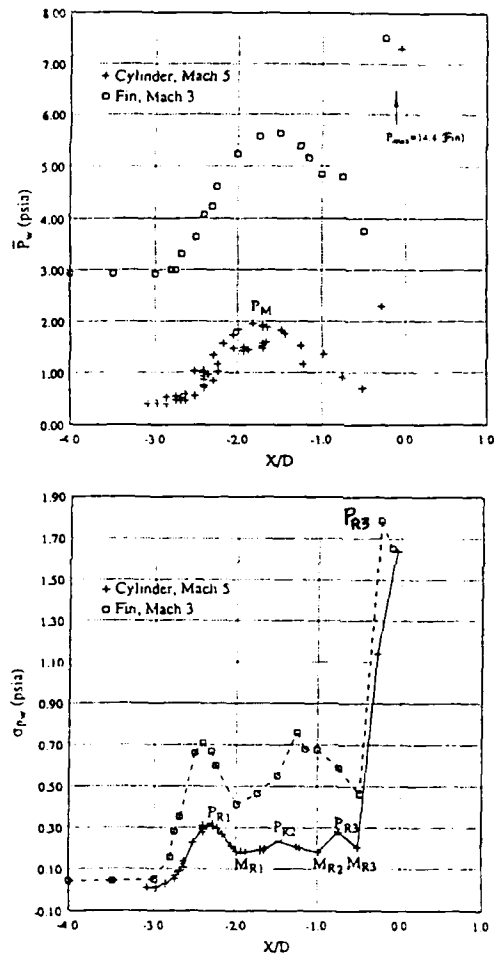
- [29] Voitenko, Zubkov, and Panov (1966), "Supersonic Gas Flow Past a Cylindrical Protuberance on a Plate," *Akademiya Nauk SSSR, Ivestiya, Mekhanika Zhidkosti i Gaza*, Vol. 1, No. 1, pp. 121-125, 1966; trans. in the Johns Hopkins University Applied Physics Laboratory Library Bulletin.
- [30] Voitenko, D.M., Zubkov, A.I., and Panov, Y.A. (1967), "Existence of Supersonic Zones in Three-Dimensional Separated Flows," *Akademiya Nauk SSSR, Ivestiya, Mekhanika Zhidkosti i Gaza*, Vol. 2, No. 1, pp. 20-24, 1967; trans. in the Johns Hopkins University Applied Physics Laboratory Library Bulletin.
- [31] Zorumski, W.E. (1987), "Fluctuating Pressure Loads Under High Speed Boundary Layers," NASA TM-100517, October 1987.

Figures

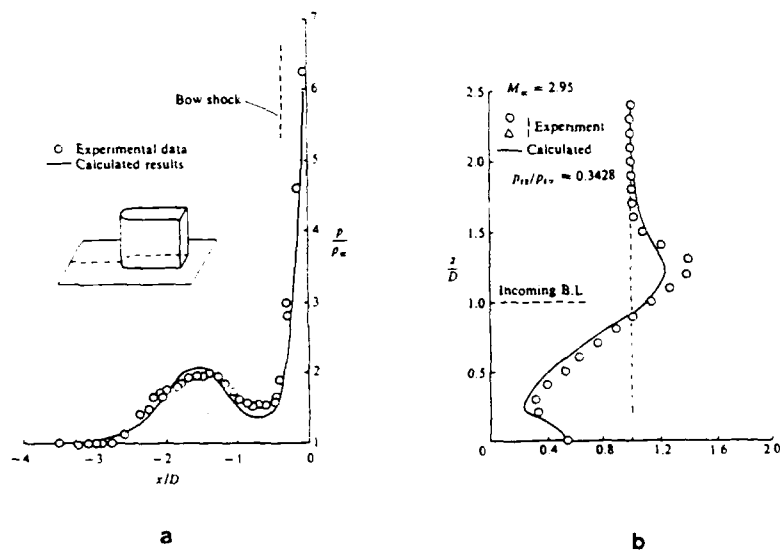


Blunt-Fin-Induced Interaction

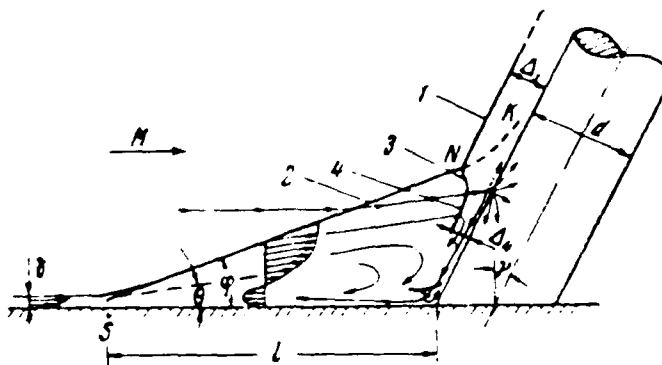
1.1 General Characteristics of Fin-Induced Shock Wave Turbulent Boundary layer Interaction (Blank, 1993)



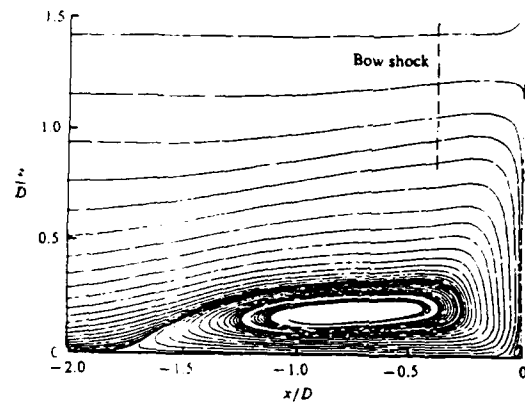
2.1 Mean and RMS Pressure Distributions on Centerline Upstream of Blunt Fins at Mach 3 and Mach 5 (Dolling, 1993)



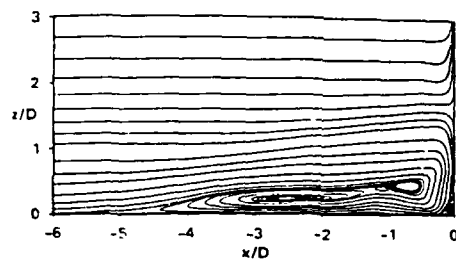
2.2 Computed Pressure Distribution at Mach 3 (a) Centerline; (b) Fin Leading Edge (Hung and Buning, 1985)



2.3 Mean Flow Field Structure (Avduevskii and Medvedev, 1967)

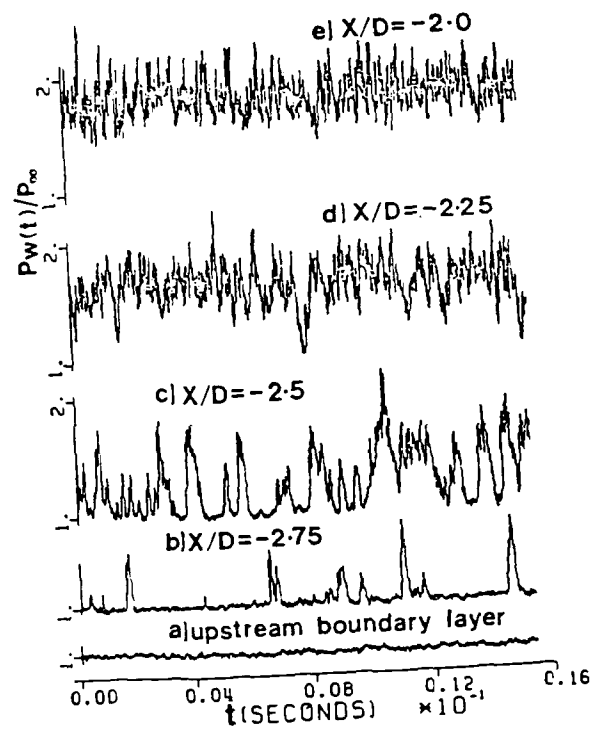


a

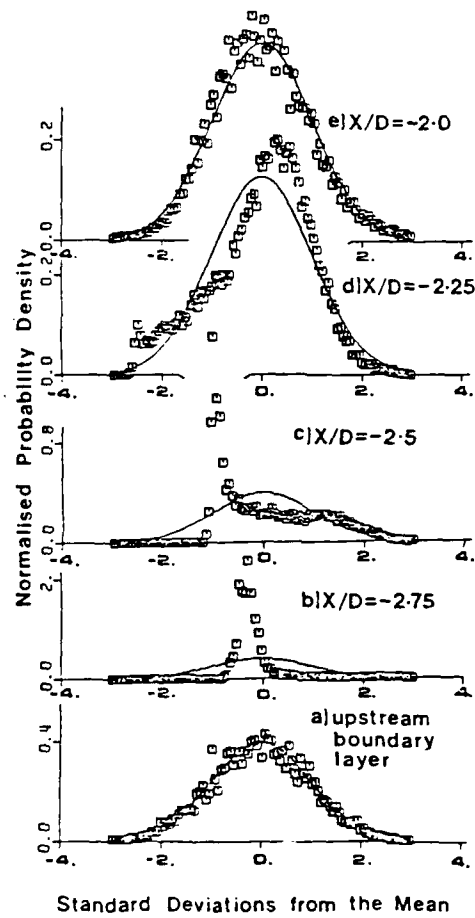


b

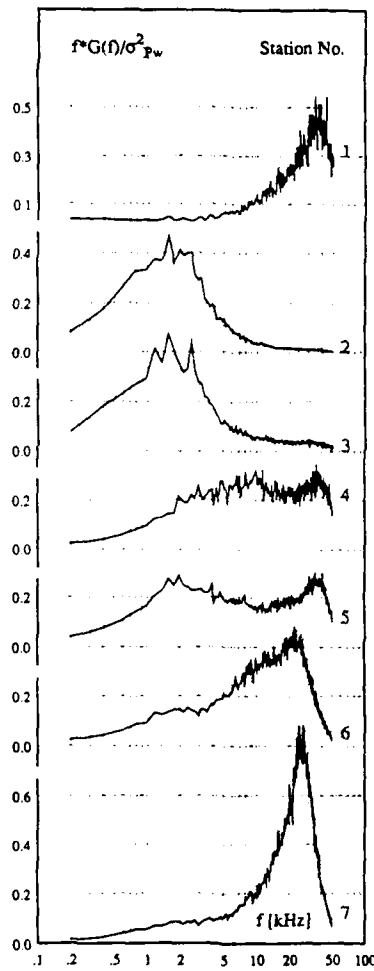
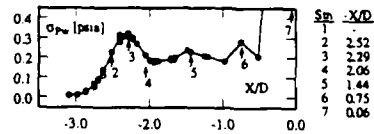
- 2.4 Computed Particle Paths in the Plane of Symmetry, (a) Mach 3 Hemicylindrically Blunted Fin (Hung and Buning, 1985), (b) Mach 5 Flat Faced Fin (Hung 1989)



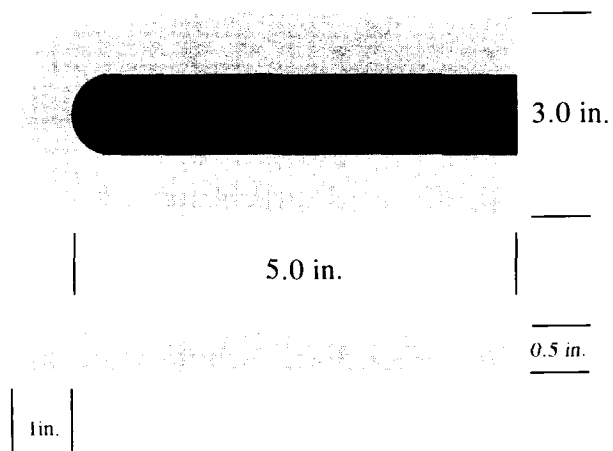
2.5 Samples of Pressure Time Histories Upstream of Fin on Centerline
(Dolling and Bogdonoff, 1981)



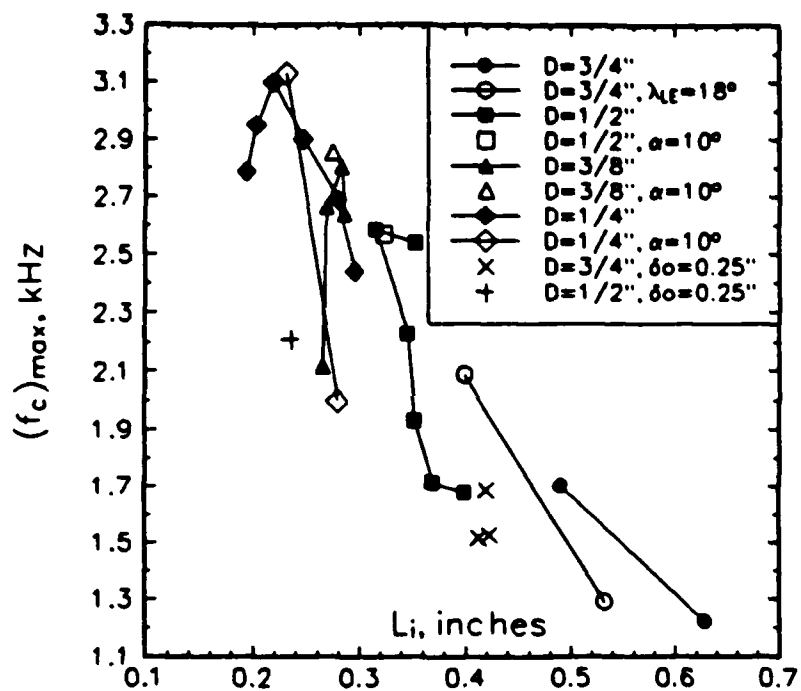
2.6 Wall Pressure Probability Density Distributions Upstream of Fin on Centerline (Dolling and Bogdonoff, 1981)



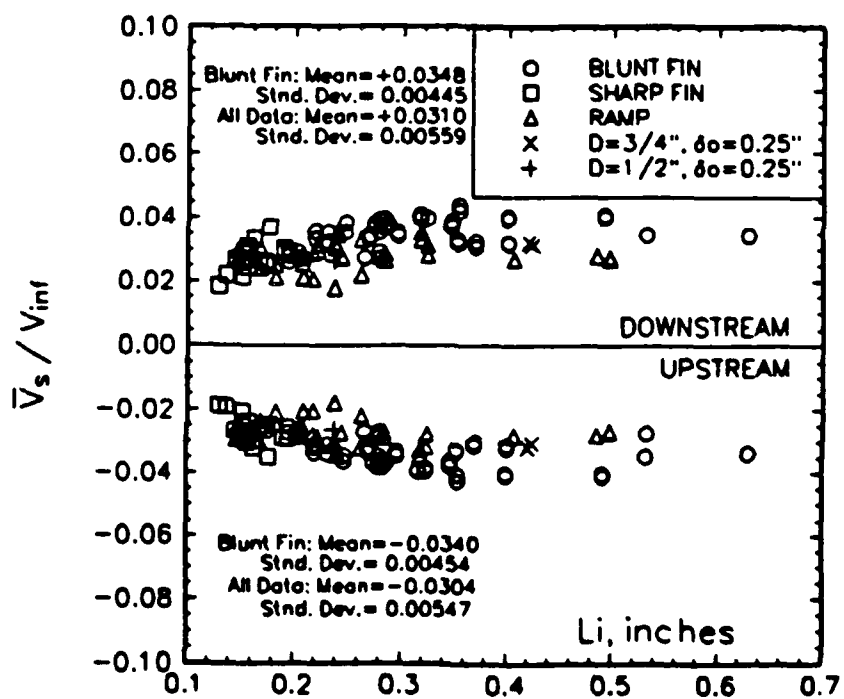
2.7 Power Spectral Density Distributions on Centerline in Mach 5 Blunt Fin Interactions (Brusniak and Dolling, 1992)



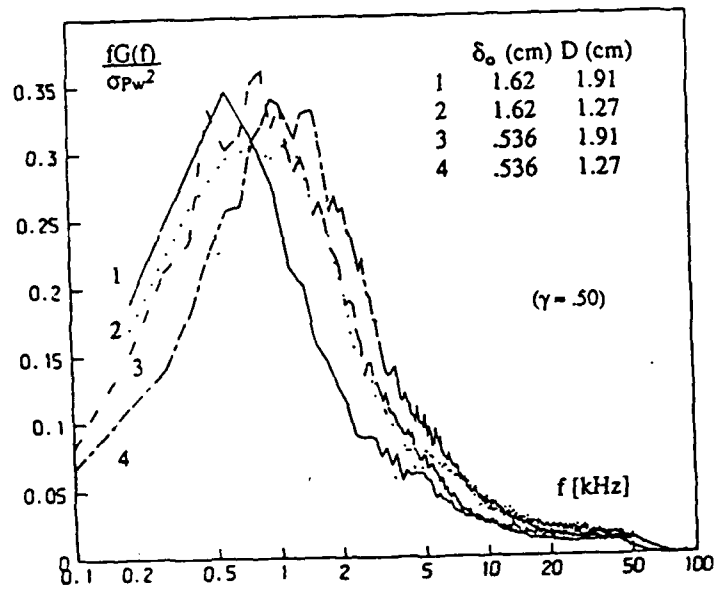
2.8 "Skirt" Fin Root Modification (Blank 1992)



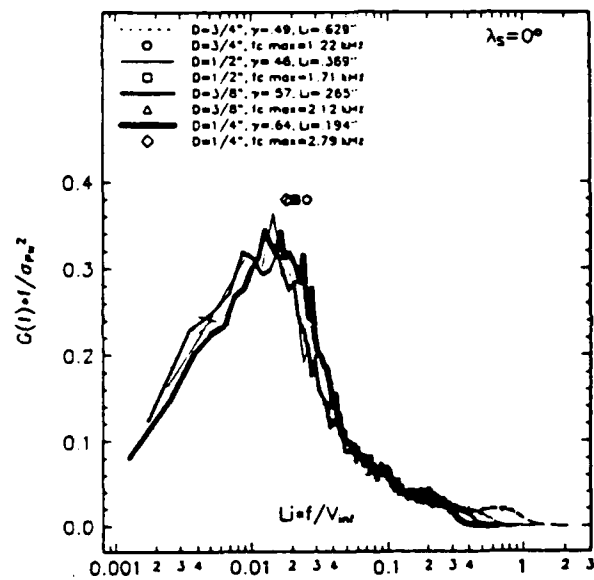
2.9 Maximum Shock Zero Crossing Frequency as a Function of Intermittent Region Length for all Model Configurations (Gonzalez and Dolling, 1993)



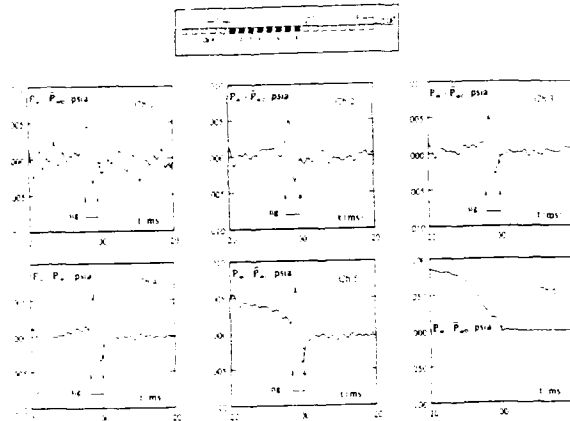
2.10 Mean Shock Velocity Normalized by Freestream Velocity as a Function of Intermittent region Length for all Model Configurations (Gonzalez and Dolling, 1993)



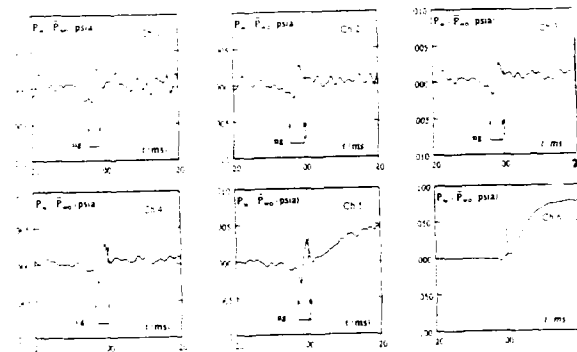
2.11 Effects of cylinder diameter and boundary layer thickness on power spectra at maximum RMS near separation in Mach 5 interactions (Dolling and Smith, 1989)



2.12 Correlation of power spectra at maximum rms near separation using L_i as a scale for the reduced frequency (Gonzalez and Dolling, 1993)

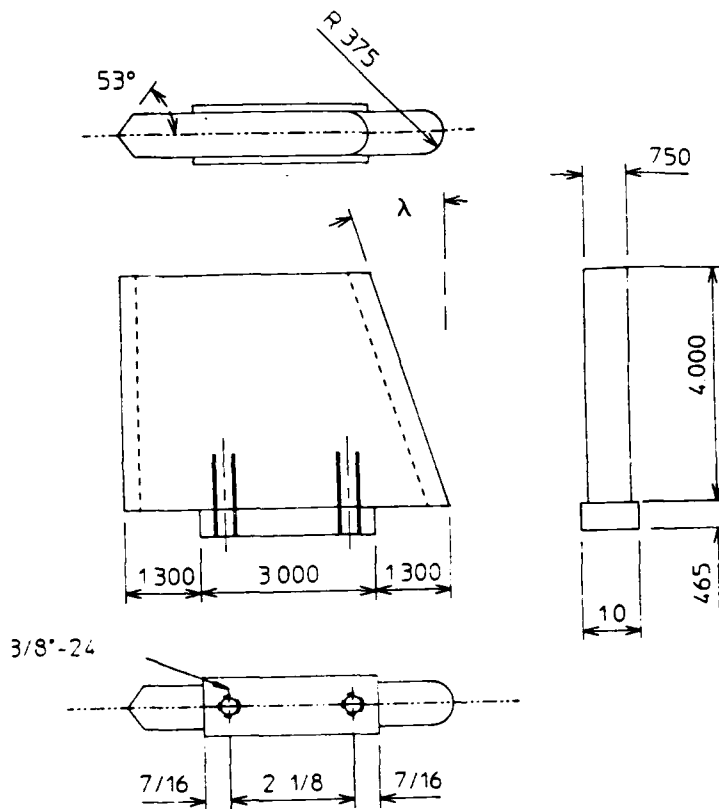


(a)

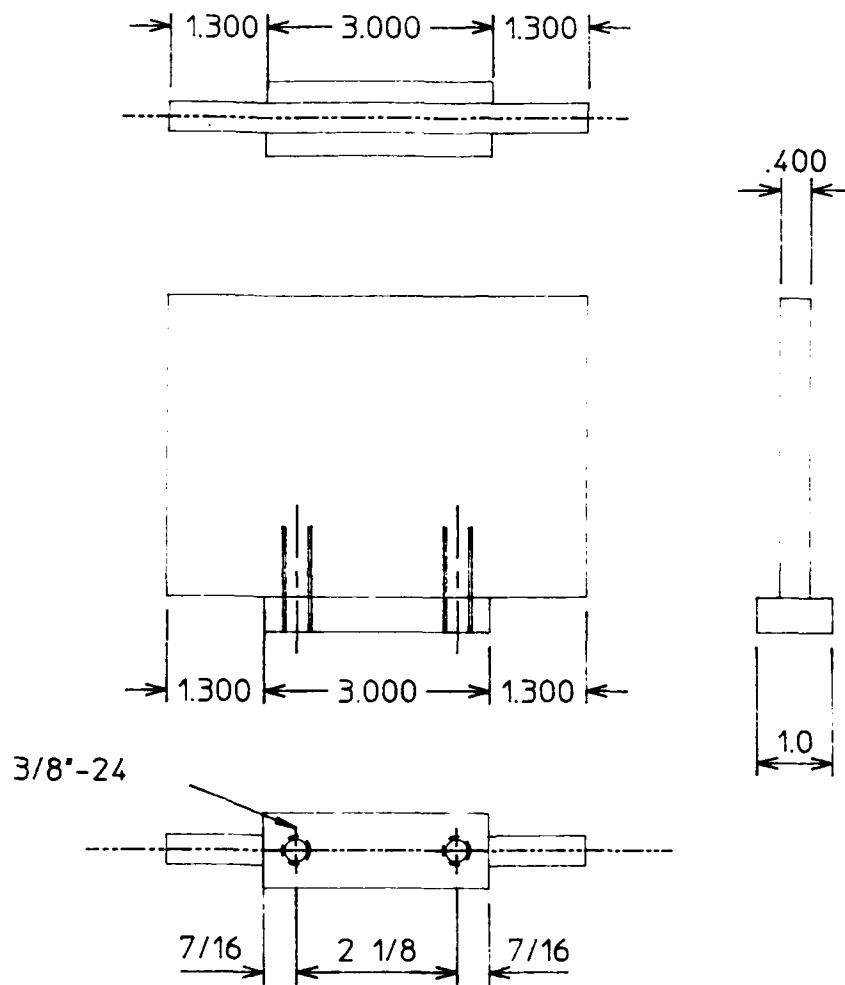


(b)

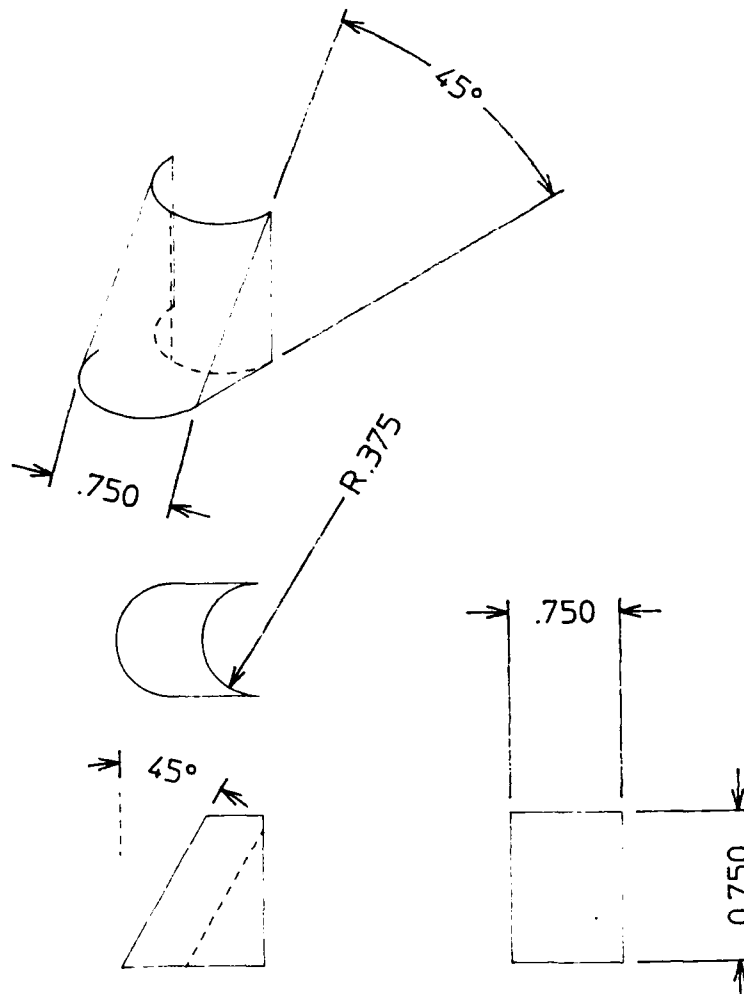
2.13 Ensemble-averaged wall pressure histories for (a) 3-channel downstream sweep, (b) 3-channel upstream sweep (trigger on channel 7) (McClure, 1992)



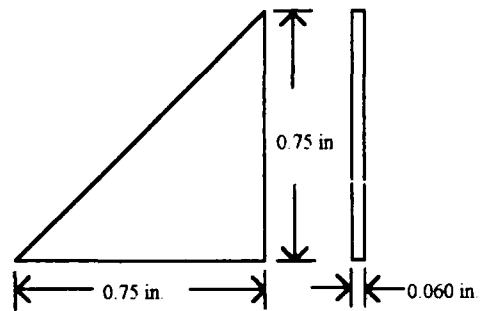
3.1 Swept Hemicylindrically Blunted Fins and Wedge Shaped Leading Edge Fin



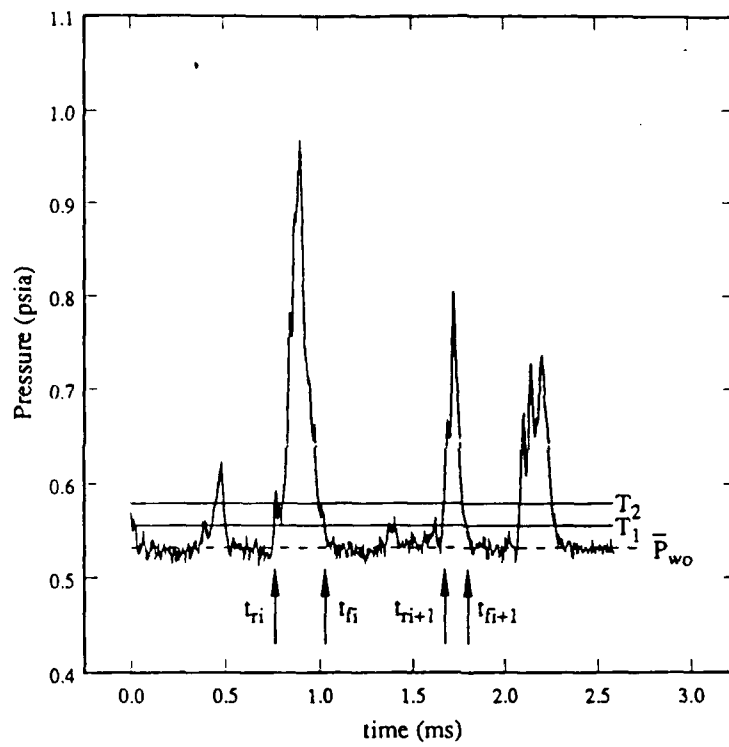
3.2 Flat Faced Fin



3.3 Swept Hemicylindrically Blunted Fillet



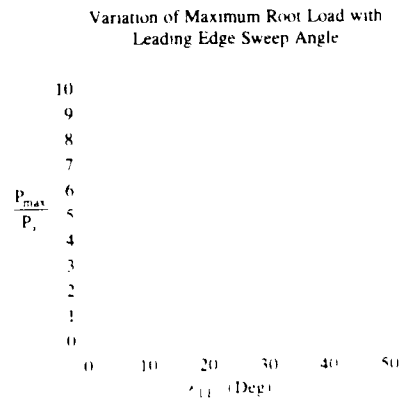
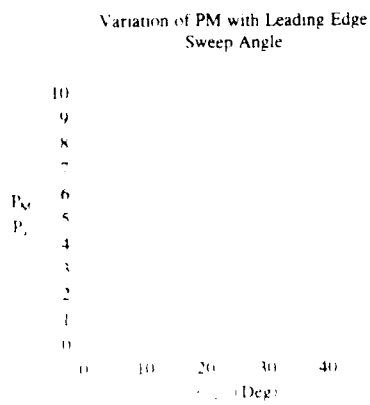
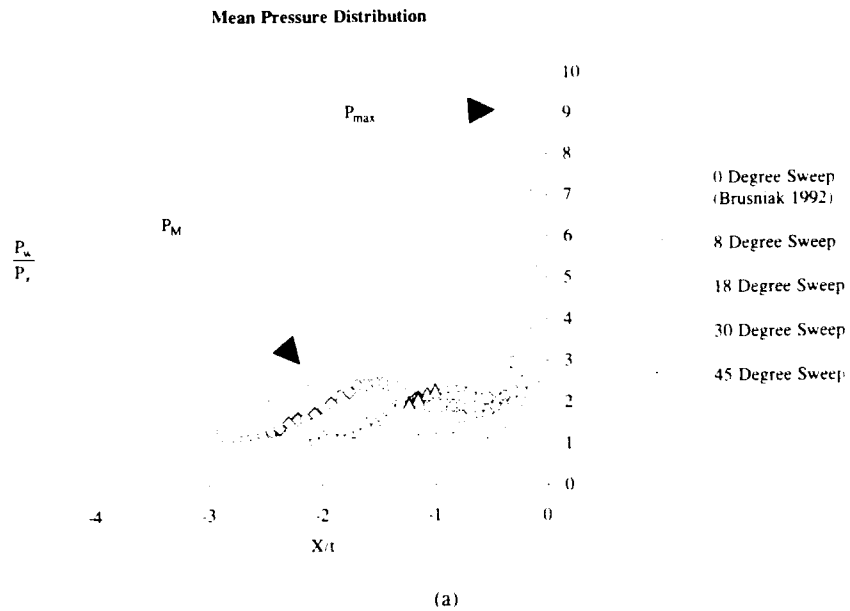
3.4 Strake Modification to Unswept Fin Root



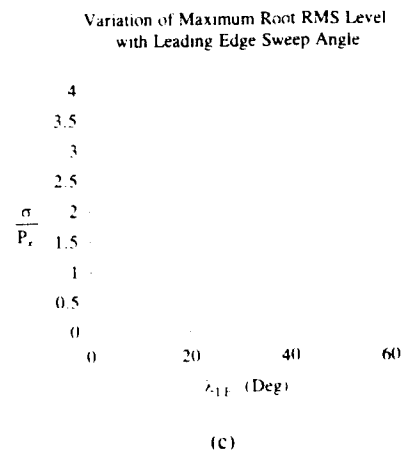
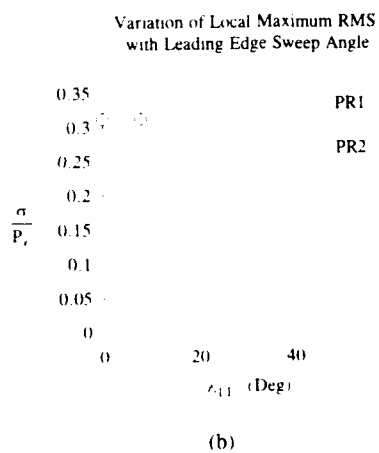
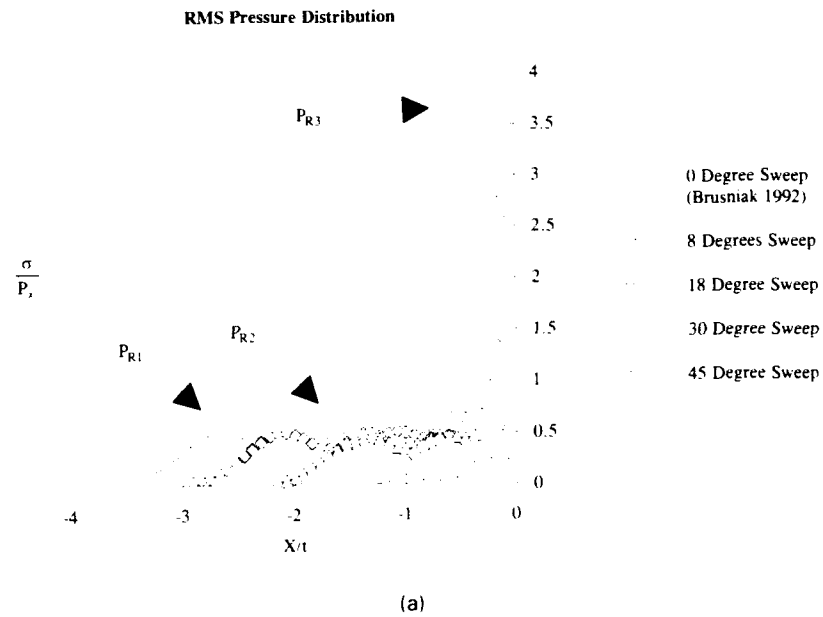
4.1 Application of the Two-Threshold Algorithm (Brusniak 1991)



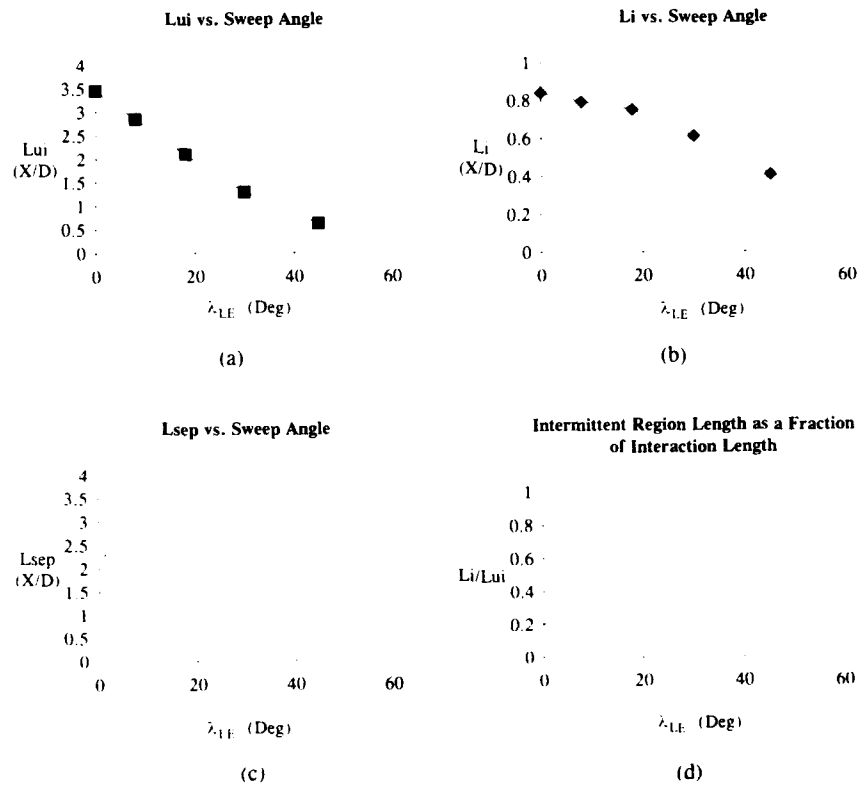
1
2
4



5.1 Variation of Mean Pressure with Leading Edge Sweep

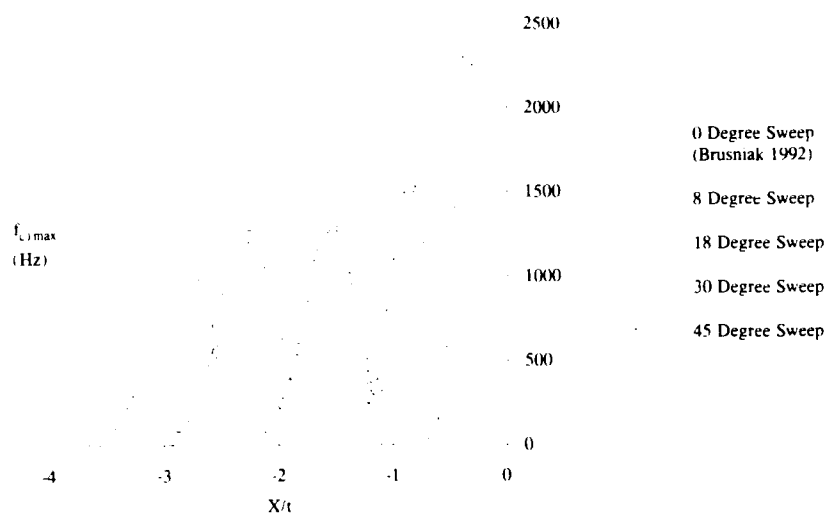


5.2 Variation of RMS Pressure with Leading Edge Sweep



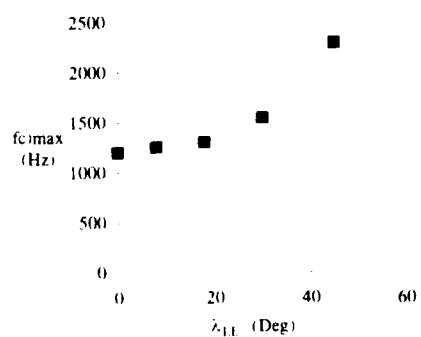
5.3 Variation of Flow Length Scales with Leading Edge Sweep

Zero-Crossing Frequency vs. Distance From Fin Leading Edge

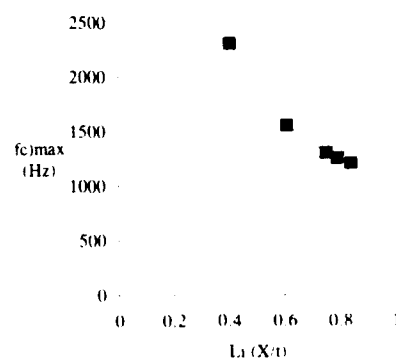


(a)

Variation of Zero-Crossing Frequency with Sweep



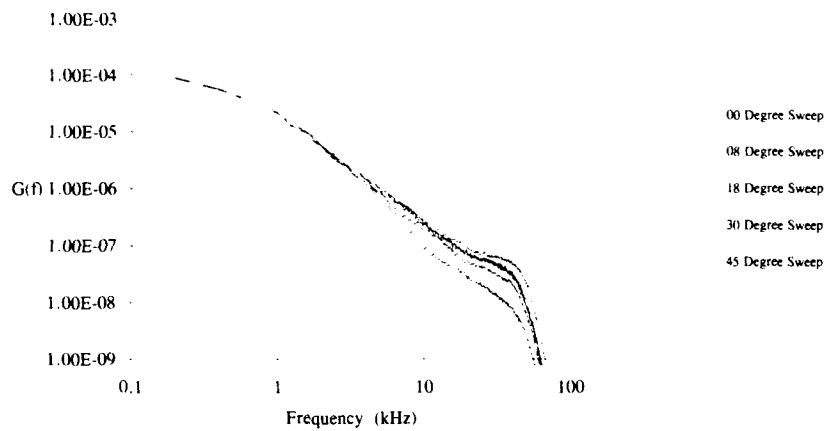
(b)

Zero-Crossing Frequency vs L_1 

(c)

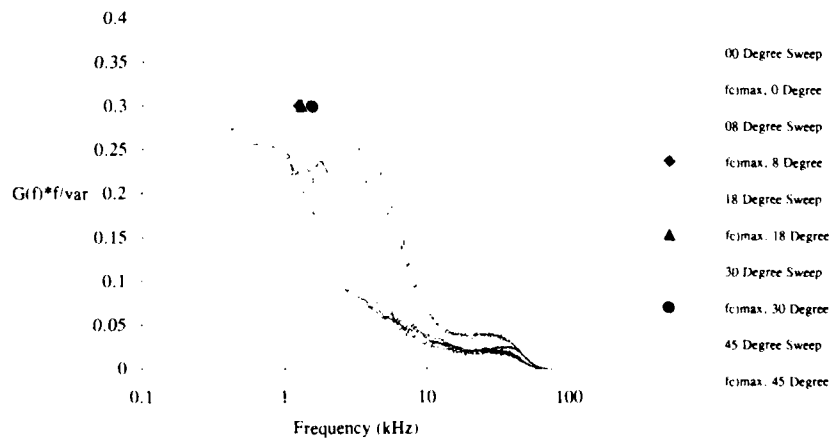
5.4 Variation of Zero-Crossing Frequency with Leading Edge Sweep

Power Spectra at 50% Intermittency



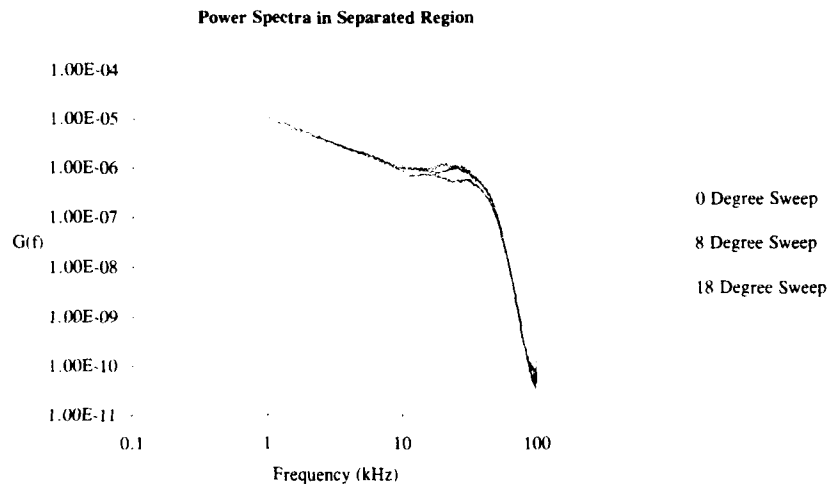
(a)

Normalized Spectra at 50% Intermittency

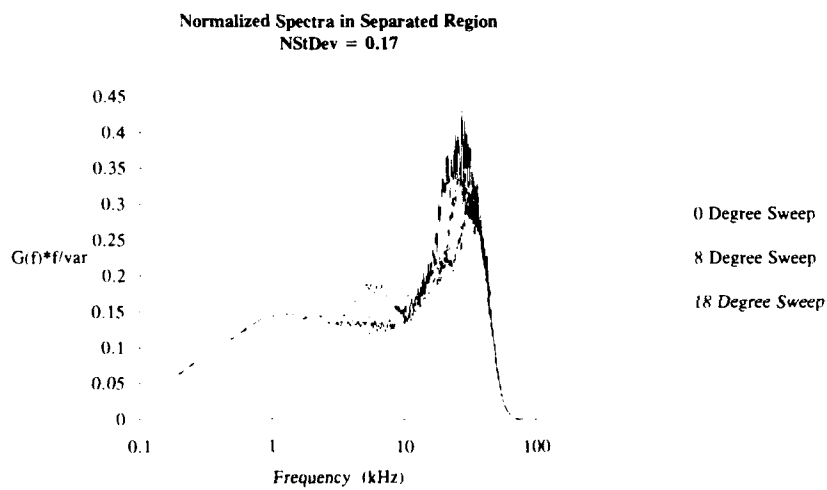


(b)

5.5 Dimensional and Normalized Power Spectral Density Distributions at 50% Intermittency

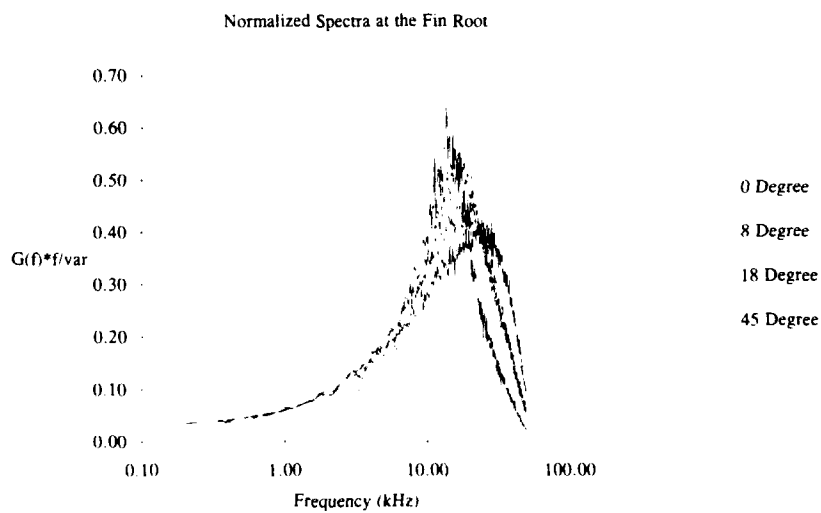
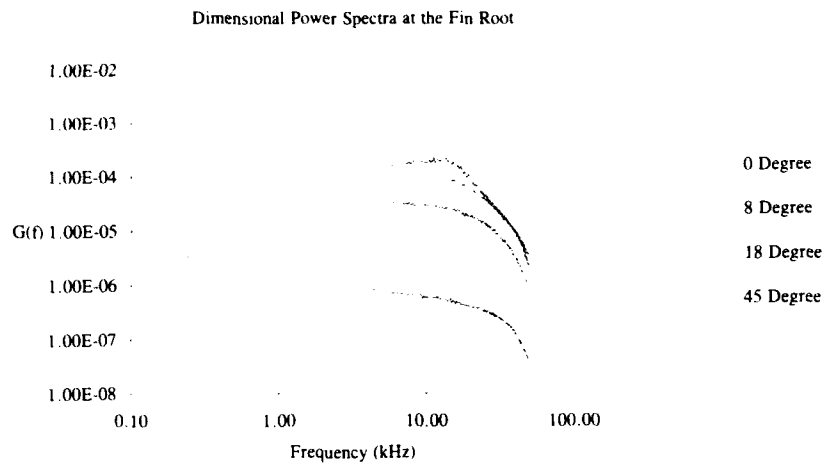


(a)



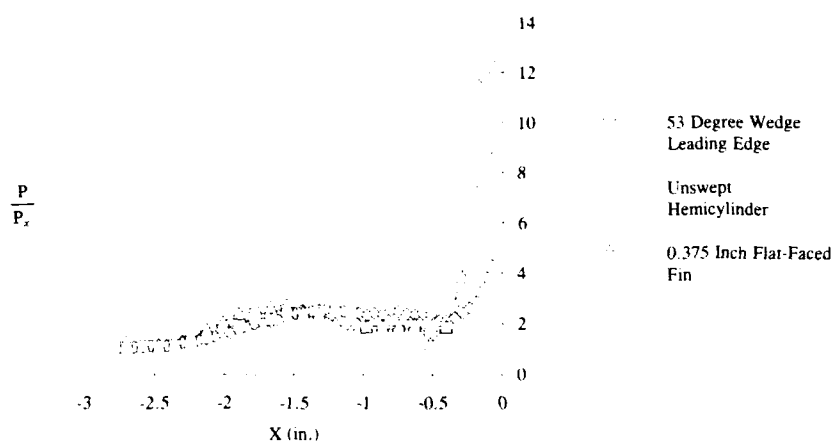
(b)

5.6 Dimensional and Normalized Power Spectral Density Distributions in the Separated Region



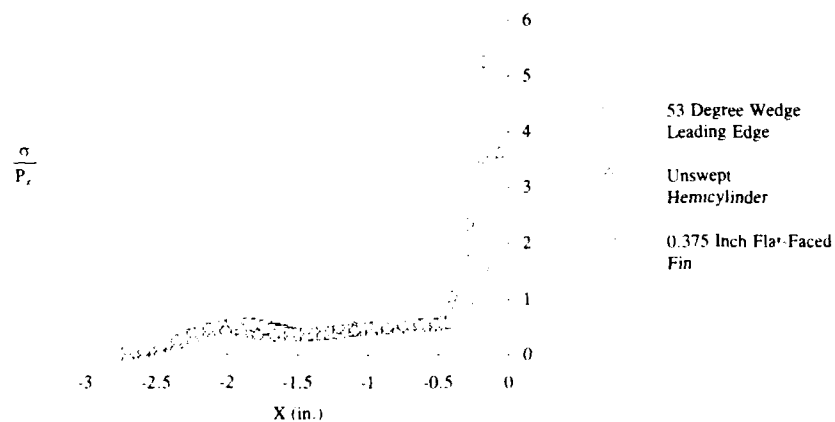
5.7 Dimensional and Normalized Power Spectral Density Distributions at the Fin Root

Mean Pressure Distribution



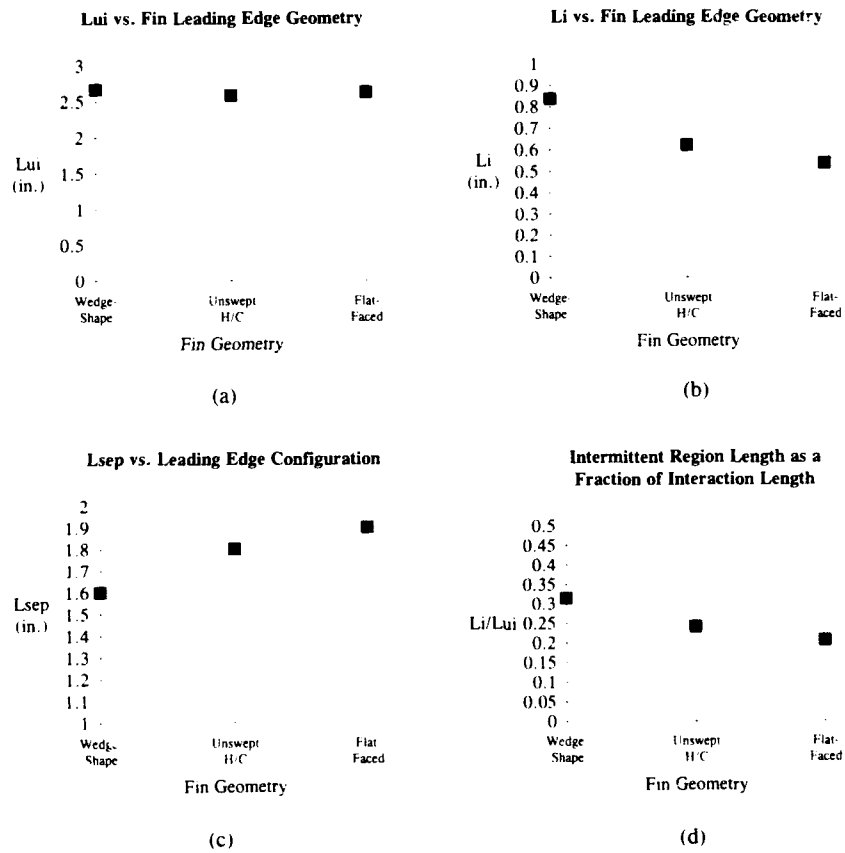
(a)

RMS Pressure Distribution



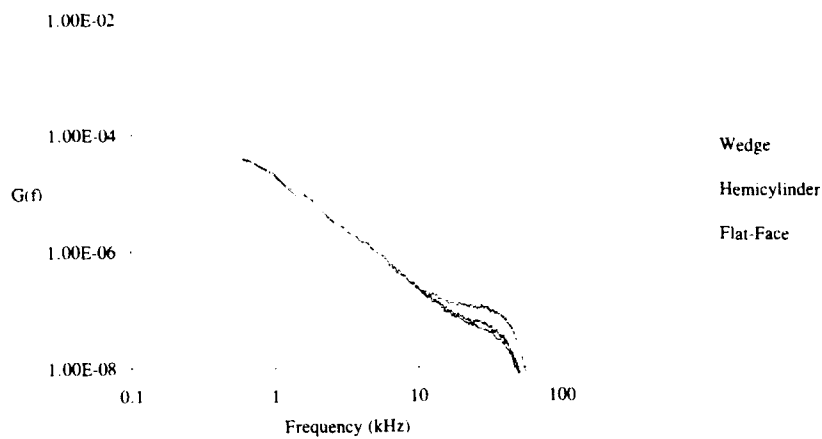
(b)

5.8 Mean and RMS Pressure Distributions for Three Interactions with the Same Upstream Influence



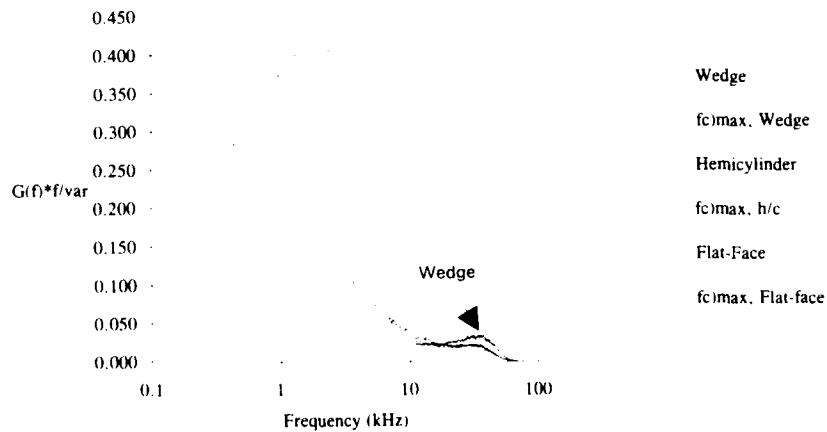
5.9 Variation of Flow Length Scales with Leading Edge Geometry

Power Spectra at 50% Intermittency



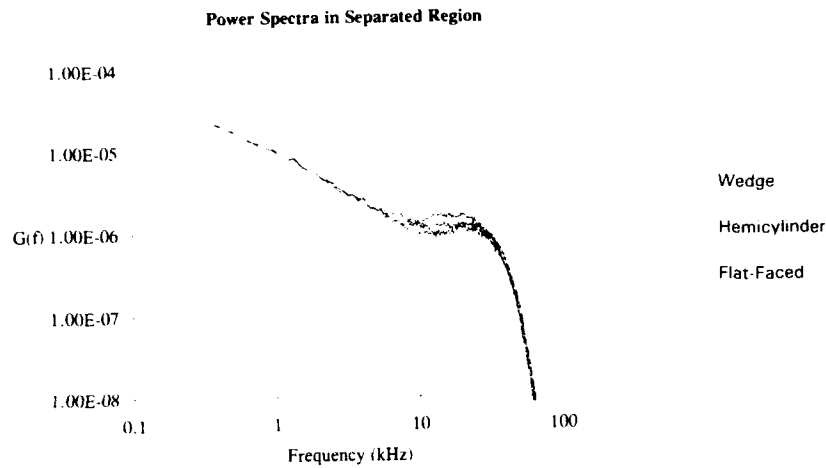
(a)

Normalized Spectra at 50% Intermittency

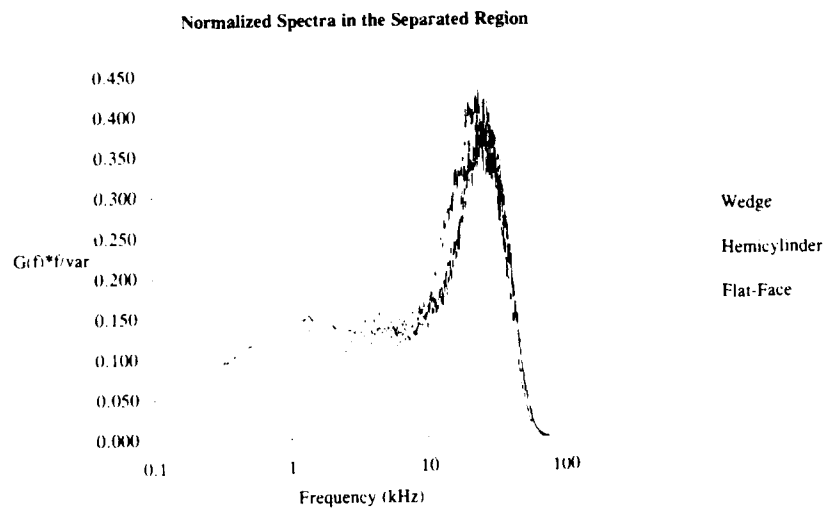


(b)

5.10 Dimensional and Normalized Power Spectral Density Distributions at 50% Intermittency

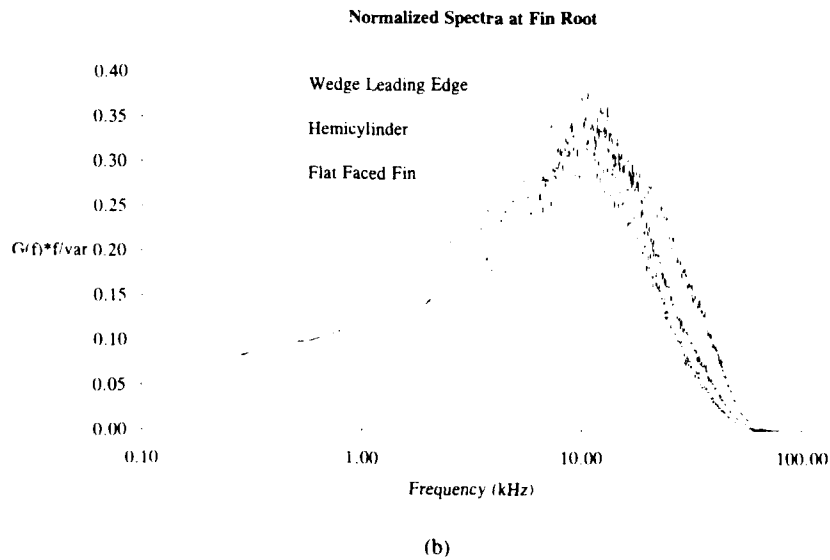
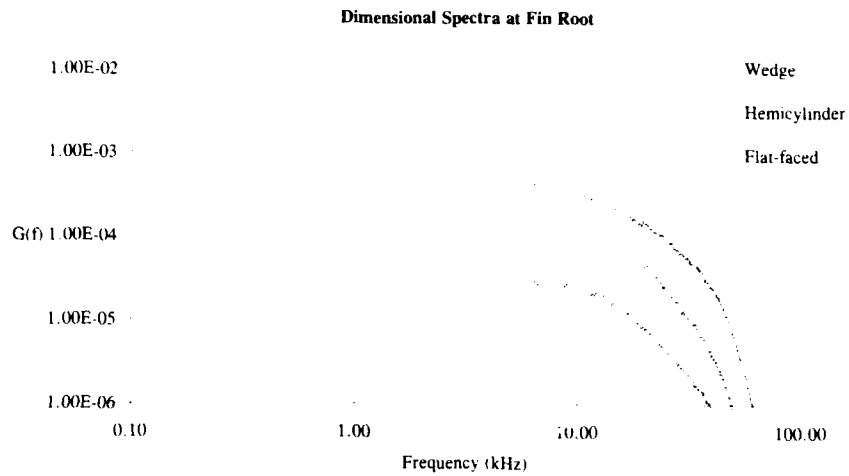


(a)

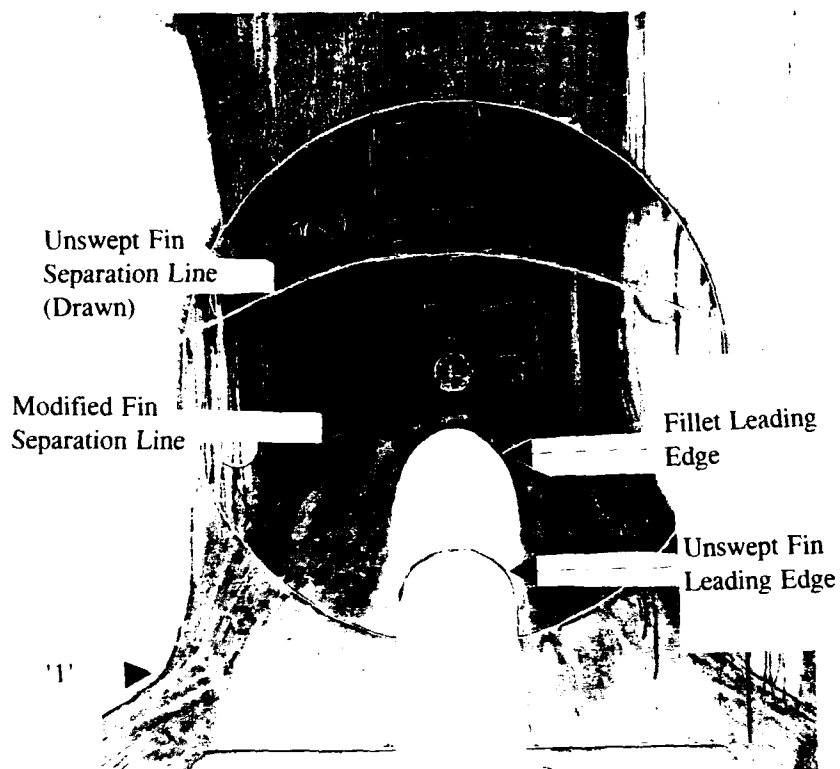


(b)

5.11 Dimensional and Normalized Power Spectral Density Distributions in the separated Region

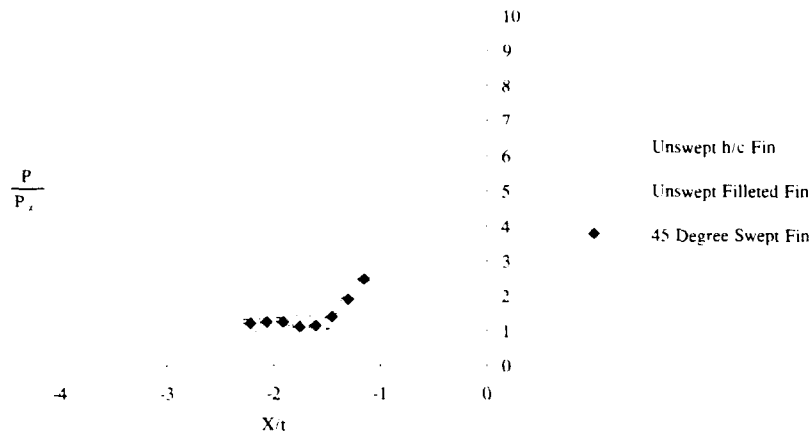


5.12 Dimensional and Normalized Power Spectral Density Distributions at the Fin Root



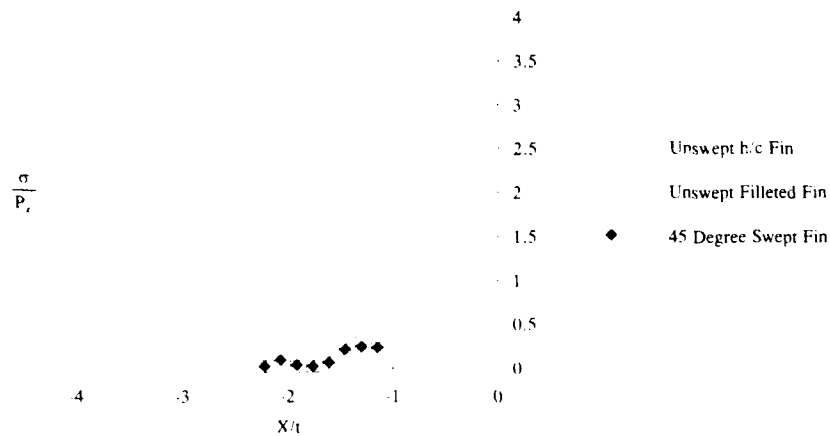
5.13 Flow Visualization Results for Unswept Hemicylindrically Blunted Fin and Unswept Fin with Fillet Root Modification

Mean Pressure Distribution



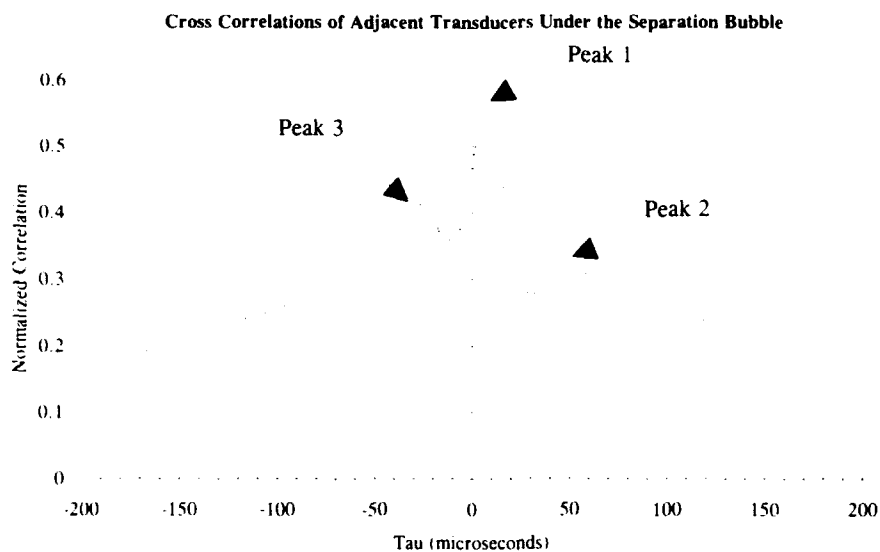
(a)

RMS Pressure Distribution

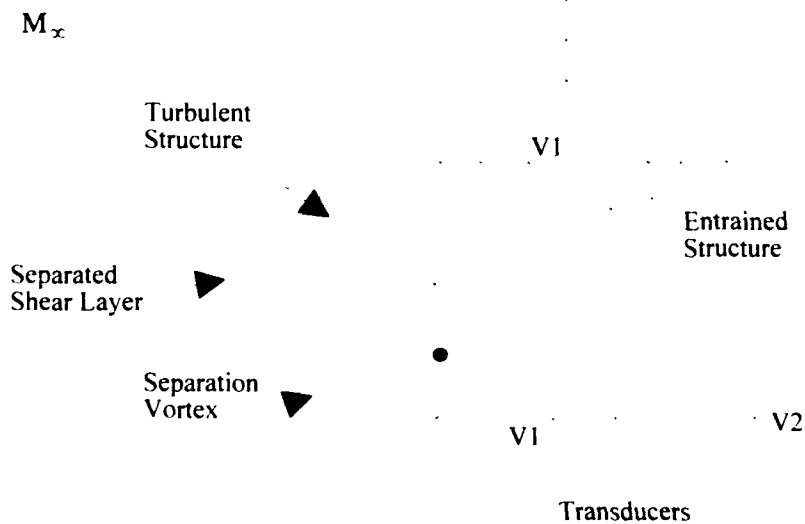


(b)

5.14 Mean and RMS Pressure Distribution for the Hemicylindrically Blunted Fillet



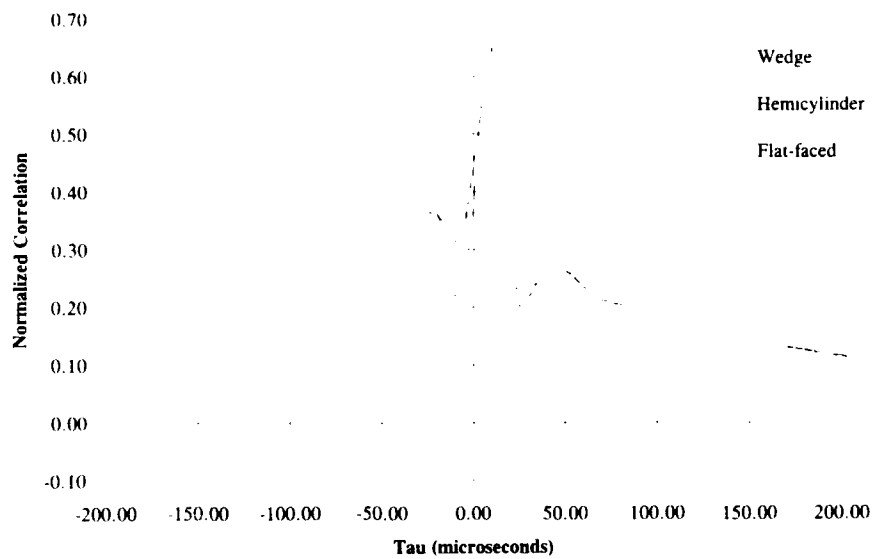
(a)



(b)

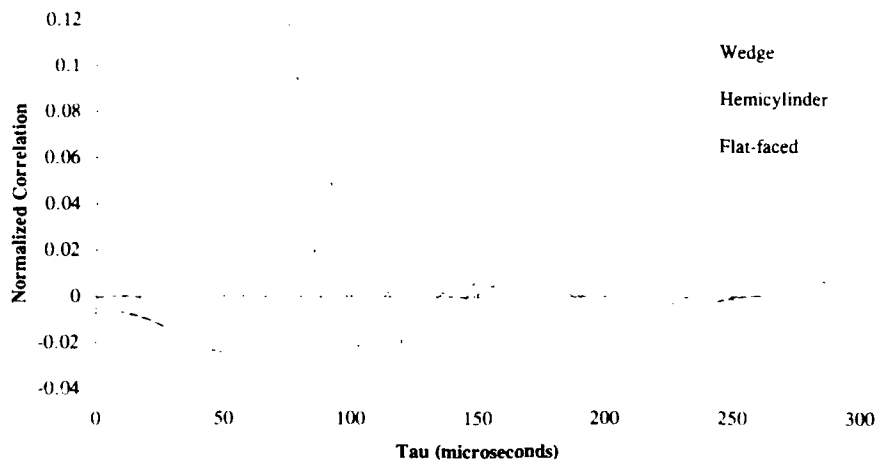
5.15 Cross Correlation of Fluctuating Pressure Measurements from Adjacent Transducers in the Separated Region

**Cross Correlation of Adjacent Transducers
at the Same Location in Different Interactions**



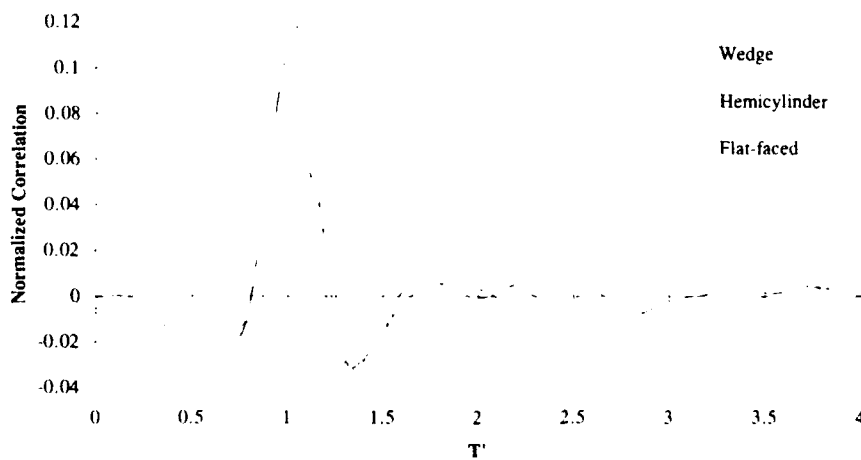
**5.16 Cross-correlation of adjacent transducers at the same relative location in
three different interactions**

Cross Correlation of Upstream and Downstream Fluctuations



(a)

Cross Correlation of Upstream and Downstream Fluctuations



(b)

5.17 Cross-correlation of signals from upstream and downstream of separation

VITA

Kelly Kleifges was born at Fort Meade, Maryland, on August 20, 1968, the son of Thomas and Jane Kleifges. After graduating valedictorian from Lakenheath American High School, Lakenheath, England, he entered the United States Air Force Academy. He graduated from the United States Air Force Academy with distinction (magna cum laude equivalent), and received the degree of Bachelor of Science in Aeronautical Engineering (with honors) with a regular commission in the U.S. Air Force in May 1990. He attended Undergraduate Pilot Training (UPT) at Reese AFB, Lubbock, Texas, and received his Certificate of Aeronautical Rating in October 1991. In January 1992 he entered The Graduate School of The University of Texas.

Permanent address: 15215 Crescent St.

Woodbridge, VA 22193

This thesis was typed by the author.